

An atlas of two-dimensional materials†

Cite this: *Chem. Soc. Rev.*, 2014, **43**, 6537

Pere Miró,* Martha Audiffred and Thomas Heine*

The discovery of graphene and other two-dimensional (2D) materials together with recent advances in exfoliation techniques have set the foundations for the manufacturing of single layered sheets from any layered 3D material. The family of 2D materials encompasses a wide selection of compositions including almost all the elements of the periodic table. This derives into a rich variety of electronic properties including metals, semimetals, insulators and semiconductors with direct and indirect band gaps ranging from ultraviolet to infrared throughout the visible range. Thus, they have the potential to play a fundamental role in the future of nanoelectronics, optoelectronics and the assembly of novel ultrathin and flexible devices. We categorize the 2D materials according to their structure, composition and electronic properties. In this review we distinguish atomically thin materials (graphene, silicene, germanene, and their saturated forms; hexagonal boron nitride; silicon carbide), rare earth, semimetals, transition metal chalcogenides and halides, and finally synthetic organic 2D materials, exemplified by 2D covalent organic frameworks. Our exhaustive data collection presented in this Atlas demonstrates the large diversity of electronic properties, including band gaps and electron mobilities. The key points of modern computational approaches applied to 2D materials are presented with special emphasis to cover their range of application, peculiarities and pitfalls.

Received 5th March 2014

DOI: 10.1039/c4cs00102h

www.rsc.org/csr

1. Introduction

During the first decades of the 20th century, the existence of two-dimensional (2D) materials was a highly debated issue in

Jacobs University Bremen, Center of Functional Nanomaterials (NanoFun), Campus Ring 1, 28759 Bremen, Germany. E-mail: p.miro@jacobs-university.de, t.heine@jacobs-university.de

† Electronic supplementary information (ESI) available: Cartesian coordinates, electronic band structures, band gaps and effective masses of electrons and holes. See DOI: 10.1039/c4cs00102h

the physics community. According to classical physics, 2D materials are thermodynamically unstable at any finite temperature due to thermal lattice fluctuations.^{1–3} This was in agreement with the decreasing melting temperature observed when the thickness of thin films was decreased. The development of modern spectroscopy revealed the existence of 3D materials with layered structure, such as graphite or molybdenum disulphide. Even though their exfoliation down to their two-dimensional monolayers was thought to be possible only in the theoretical domain since Mermin demonstrated that strictly one- and two-dimensional



Pere Miró

Pere Miró graduated from Universitat Rovira i Virgili in 2005 with a BS in Chemistry. He completed his PhD under the supervision of Prof. Carles Bo at the Institute of Chemical Research of Catalonia (ICIQ) in 2010. After a postdoc at University of Minnesota under the supervision of Prof. Christopher J. Cramer, he joined Prof. Thomas Heine's group to study 2D layered materials. His research interests include low dimensionality and porous nanomaterials for nanoelectronics and catalytical applications.



Martha Audiffred

Martha Audiffred completed her PhD under the supervision of Gabriel Merino in Universidad de Guanajuato in 2013. She is currently working as a postdoctoral fellow in Prof. Thomas Heine's group. Her research interests include synthesis and theoretical characterization of low dimensional nanomaterials.

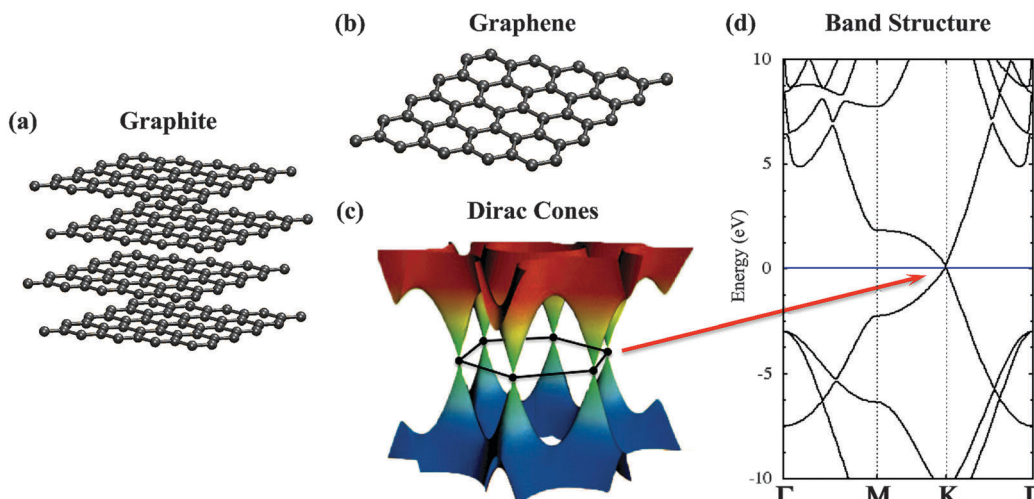


Fig. 1 Graphene, the prototype 2D material. (a) Graphite structure ($5 \times 5 \times 2$ unit cells). (b) Graphene structure (5×5). (c) Dirac cones in graphene (adopted from ref. 6). (d) Graphene band structure (Γ -M-K- Γ). Fermi level has been shifted to 0 eV and depicted with a blue horizontal line.

materials can only exist hypothetically – *i.e.* if the crystal is described within the harmonic approximation.⁴

Materials science had a major scientific breakthrough in 2004, when Novoselov and Geim isolated the first single layer 2D material, graphene, through the Scotch tape exfoliation of graphite (Fig. 1a).⁵ The importance of this achievement was sealed in 2010, when the Nobel price was awarded to both researchers.

Graphene is an atomically thin sp² carbon layered material with a honeycomb lattice that has almost the same crystal energy as diamond. As each graphene carbon has only three bonds instead of four for diamond, the graphene C-C bonds are about 25% stronger. Thus, it is the most stable material known to date. Graphene has a peculiar electronic structure. It is a semi-metal, characterized by the fact that it does not show a band gap, but the density-of-states is zero at the Fermi level. The Fermi level is crossed by electronic bands near the six corners of the two-dimensional hexagonal Brillouin zone (Fig. 1c). The dispersion relation (the change of electron energy of a band

within the Brillouin zone) is linear at these points, a unique feature that leads to zero effective mass for electrons and holes, and thus to very high currents. Due to this linear or conical dispersion relation, electrons and holes near these six points behave like relativistic particles described by the Dirac equation. Therefore, the electrons and holes are called Dirac fermions and the six corners of the Brillouin zone are called the Dirac points. The cones at Dirac points are located at the high-symmetry **K** points in the Brillouin zone of the honeycomb lattice and have been recently explored towards valleytronics applications (Fig. 1c and d). The massless Dirac electrons at the Fermi level derive also in the highest known finite-temperature electron mobility. Furthermore, the extremely low spin-orbit (SO) interaction in graphene makes it an ideal spin carrier for spintronics.⁶ Research on electronic structure engineering of graphene rapidly emerged to the development of semiconducting modifications exhibiting a (very) low band gap, an important step towards electronic and optoelectronic applications. However, these devices require larger band gap semiconductors and dielectric materials as insulators. Luckily, nature offers a manifold of layered materials beyond graphene, including metals, semimetals, insulators and semiconductors with direct and indirect band gaps ranging from ultraviolet to infrared through the visible range.

The recent progress in exfoliation techniques such as micro-mechanical cleavage, ion intercalation, and surfactant-assisted ultrasonication has set the foundations for the manufacturing of essentially any given layered bulk material in the monolayer limit.^{7,8} Layered materials cover an extremely large range of compounds, including clays, layered oxides, chalcogenides, halides, carbides, nitrides, hydrides, hydroxides, phosphates and phosphonates. Most of these materials are binary layered compounds although ternary layered compounds are also possible (*i.e.* CuSbS₂).⁹ Layered materials can be further classified based on the nature of the interaction between the layers. This interaction is governed by hydrogen bonds, interstitial



Thomas Heine

Thomas Heine graduated from TU Dresden and, after postdoctoral stages in Bologna, Exeter and Dresden became Associated (2008) and Full (2011) Professor of Theoretical Physics/Theoretical Materials Science at Jacobs University Bremen. His research interests include the development of methods and software for materials science, molecular framework compounds, 2D inorganic materials and theoretical spectroscopy.

cations or London dispersion interactions between the layers. Among the latter, transition metal chalcogenides (TMC) are the most prominent examples of these materials with MoS₂ as its flagship.^{10–13} Indeed, the development of MoS₂ based transistors has triggered an immense scientific interest in TMC monolayers for novel ultrathin and flexible devices as well as for other nanoelectronic and optoelectronic applications.^{14,15}

Besides the immense success of 2D materials science one should not forget the underlying physics. According to all theoretical predictions, 2D materials should not exist above absolute zero.^{1–4} The study of free standing and supported graphene revealed the formation of intrinsic ripples. These findings were also corroborated through theoretical studies on free-standing graphene sheets.^{16,17} Thus, on the large length scale, ripples distort the 2D lattice, making it – strictly speaking – a 3D material and thus resolving the controversy about the existence of these materials beyond absolute zero. Analogously, spontaneous ripple formation has been observed in free-standing single layer MoS₂ sheets, even though the material is not atomically thin and thus not strictly two-dimensional.^{18,19}

In this review we will discuss the fundamental electronic properties of single-layer 2D materials with special emphasis on their range of application, on their peculiarities and on pitfalls in the theoretical description of their electronic structure. The computational treatment of 2D materials requires special care when choosing the boundary conditions since these systems are infinite in two dimensions, but finite in the third. Furthermore, the exfoliation down to the monolayer has implications in the final properties of these materials. The most intriguing paradigm change is certainly the appearance of the massless Dirac Fermions in graphene.²⁰ Another one is the appearance of the giant spin orbit splitting in MoS₂.^{21,22,99} Additionally, due to their 2D character, the determination of band structures requires special attention; as due to a quenched screening of the Coulomb interaction a strong exciton binding energy is present. This has a strong impact on quasi-particle approaches such as GW theory.^{23,24}

In the light of the scarce and not systematic data on the electronic properties of a representative fraction of single-layer 2D materials in the literature (Fig. 2), we have computed this data at a consistent level of theory (density-functional theory and approximate quasi-particle theory). These results are presented in this article and compared with previous experimental and theoretical results whenever available. The studied materials include atomically thin 2D materials, starting with graphene and direct analogues such as hexagonal boron nitride (*h*-BN), silicon carbide (SiC), silicene and germanene as well as their hydrogenated and halogenated derivatives. Further, we present exfoliated monolayer structures of transition metal chalcogenides (TMCs), semimetal chalcogenides (SMCs), and transition metal halides (TMHs) including M'X, M₂N, MX₂, MY₂, MY₃ (M' = Ga and In; M = Ti, Zr, Hf, Nb, Mo, W, Re, Pd, Pt, etc.; X = S, Se and Te; Y = Cl, Br and I). Finally, we address an emerging family of metal-free layered organic materials with honeycomb lattice, in particular the recently reported 2D covalent organic frameworks (COFs).²⁵ Only selected examples are presented in the text, but a complete compilation of results, including geometries,

band structures, band gaps and effective masses, are presented in ESI.†

2. Methodology

A 2D material can be described as a hybrid between a solid (in the periodic plane) and a molecule (perpendicular to it). Accordingly, and as in any quantum mechanical system, the choice of the boundary conditions is crucial to properly describe the system properties. Explicit consideration of 2D periodic boundary conditions is possible if local basis functions are used. Those are implemented, for example, in CRYSTAL,²⁶ SIESTA^{27,28} and ADF/BAND software.^{29–31}

Modeling a 2D system as finite cluster is not recommended since it is experimentally well-known that lateral quantum confinement effects arise for particle sizes below 100 nm.¹³² On the contrary, calculations using solid state codes employing the repeated slab method have become a common approach, as they allow the employment of plane-wave basis functions that are known to be computationally very efficient and are hence widely used in physics. Popular codes include Quantum-Espresso,³² abinit,^{33–35} and VASP.^{36–38} Plane wave basis functions span the full 3D simulation box and hence require a vacuum layer such that there is no spurious self-interaction between the studied system and its periodic images in the direction perpendicular to the 2D lattice plane. This is fundamental since even though the interlayer interaction is weak, it has significant impact on the electronic structure. For example, band gaps may double from bulk to monolayer, as known for many transition metal dichalcogenides,³⁹ or the character of the material may change from semiconducting to metallic, as in graphene⁴⁰ or palladium sulphide.⁴¹ Thus, when using the repeated slab method, the convergence of the results must be checked with respect to the extension of the vacuum layer, as indicated in Table 1. It is worth to note that plane-wave methods scale with the size of the simulation box, therefore, as commonly known from solid state physics, their efficiency is reduced in case of the calculation of single layered materials. As result, 2D materials are faster processed (per atom and compared to their bulk counterparts) if using explicit 2D boundary conditions, due to the reduced complexity of interactions per atom, while they slow down calculations using 3D boundary conditions and plane waves (Table 1).

Almost all elements of the periodic table have been incorporated as main components in 2D materials or as dopants. Thus, high quality basis sets for a large number of elements are required. It is popular to reduce computational complexity and cost by replacing core electrons by pseudo potentials (PP) or effective core potentials (ECPs). It should be reminded that a careful validation of those numerical treatments is required, as they can have a significant effect on computed quantities such as band gaps and band structures. Furthermore, relativistic effects have found to be important even for relatively light-weight elements in several 2D materials. The inclusion of relativistic effects for core electrons is achieved either by including them

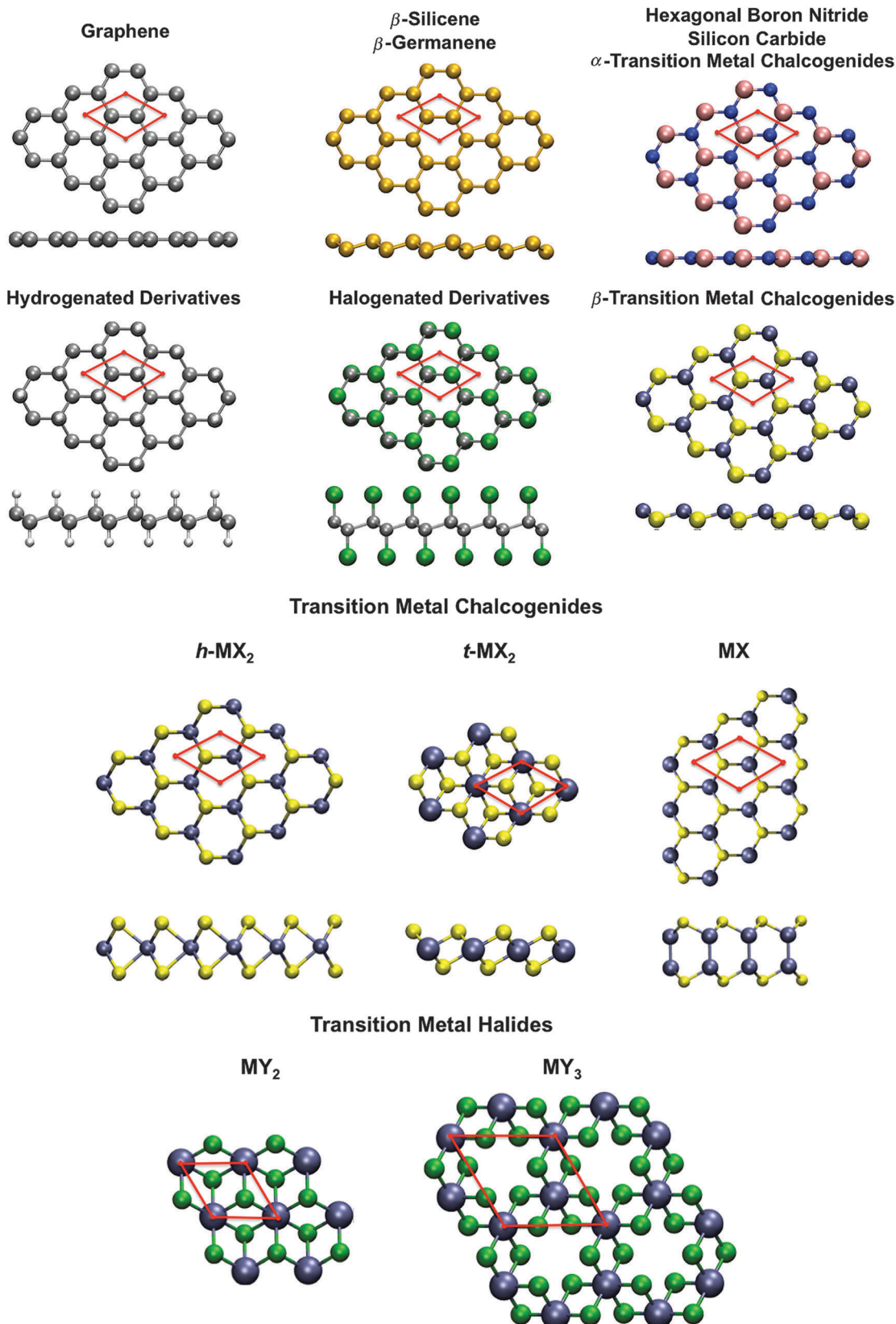


Fig. 2 Structure of atomically thin 2D materials: graphene, silicene, germanene (and their derivatives), silicon carbide (SiC), hexagonal boron nitride (h -BN) and transition metal chalcogenides (TMC) (top). Ultrathin 2D materials such as transition metal chalcogenides (TMC) (centre) and halides (TMH) (bottom). Unit cells are depicted in red. Colour code: metals in ice blue, halides in green, chalcogenides in yellow, nitrogen in blue, carbon in grey, silicon and germanium in gold, boron in pink and hydrogen in white.

Table 1 Relative CPU time and electronic band gaps for graphene and MoS₂ calculated using explicit 2D periodic boundary conditions (PBC) and the repeated slab method (3D PBC). For the latter, the interlayer distance has been increased stepwise (0.4 Å) starting from the bulk value. The table shows the relative computer time with respect to the bulk system (same software, same computer). 2D PBC calculations have been carried out using local basis functions (ADF/BAND) and plane waves (VASP). All calculations employ the PBE functional. ADF/BAND calculations as specified in the Computational details. For VASP calculations an energy cutoff of 400 eV was used. Brillouin zone is sampled with a mesh of 20 × 20 × 1 (16 × 16 × 1) \mathbf{k} points for graphene (MoS₂)

Interlayer displacement ^b (Å)	Graphene		MoS ₂		Band gap (eV)	
	Relative CPU time ^a		Relative CPU time ^a		2D PBC	3D PBC
	2D PBC	3D PBC	2D PBC	3D PBC	2D PBC	3D PBC
0.0	1.00	1.00	1.00	1.00	0.89 (indirect)	0.89 (indirect)
0.4	—	1.05	—	1.11	1.22 (indirect)	1.23 (indirect)
0.8	—	1.09	—	1.18	1.46 (indirect)	1.49 (indirect)
1.2	—	1.08	—	1.17	1.64 (indirect)	1.68 (indirect)
1.8	—	1.19	—	1.33	1.77 (indirect)	1.81 (indirect)
2.4	—	1.38	—	1.35	1.82 (direct)	1.89 (indirect)
2.8	—	1.47	—	1.39	1.82 (direct)	1.91 (direct)
3.2	—	1.52	—	1.63	1.82 (direct)	1.91 (direct)
∞^c	0.32	—	0.27	—	1.82 (direct)	—

^a Total CPU time relative to bulk calculation. ^b Respect to the bulk interlayer distance. ^c 2D periodic boundary conditions.

into PPs/ECPs or by treating them explicitly through, for example, the zeroth order regular approximation (ZORA).^{42–46} Spin Orbit (SO) effects are surprisingly large for single layered 2D materials due to the break of the inversion symmetry from bulk/bilayer to the monolayer. For example, the SO induced splitting of the valence band in MoS₂ is *ca.* 150 meV at the K point which is marking the valence band maximum.²² Density-functional theory (DFT) has become the working horse of modern solid state physics as a method with a reasonable balance between accuracy and computational cost.⁴⁷ However, some points need to be raised before studying 2D materials using this method. First, on a general basis, DFT is not adequate to describe systems exhibiting strong electron correlations, as it tends to over-delocalize the electron density. The use of hybrid DFT functionals, which incorporate a fraction of the exact exchange interaction, improves this situation, but only solves this problem partially.⁴⁸ Therefore, a commonly adopted strategy is the comparison of band structures obtained by pure and hybrid GGA functionals, as for example PBE and PBE0.^{49–51} On one hand, band structures obtained at the DFT level of theory are typically of excellent quality, allowing the determination of effective masses of holes (h^+) and electrons (e^-), or the parameterization of effective Hamiltonians for multiscale transport simulations.⁵² On the other hand, DFT is known to incorrectly describe band gaps, a consequence that unoccupied Kohn–Sham orbitals are rather a mathematical result with a lack of a clear physical meaning. However, experience has proven that DFT yields a reasonable spectrum of the conduction bands when using an orbital basis with sufficient quality, but they are shifted to lower energies. In consequence, DFT band gaps are typically strongly underestimated, with notable extreme cases such as Mott insulators, where DFT predicts metallic character. Hybrid DFT functionals such as HSE06 or PBE0 improve in general the predicted band gap when compared with experimentally determined ones.^{48,53} However, hybrid functionals are computationally expensive compared with GGA ones, especially if used together with plane waves as basis functions.

A more rigorous calculation of band gaps is possible using the GW approximation, which is usually applied on top of DFT calculations.^{23,24} While it is known to produce excellent results in 3D solids, surprisingly, this approach overestimates the band gap in 2D materials. The reason for this behavior has been identified as the reduced Coulomb screening in 2D systems, which results in high exciton binding energies. For example, PBE calculations on MoS₂ monolayers yield a band gap of 1.8 eV, in very good agreement with the experimentally determined value.³⁹ On the contrary, the GW approximation yields a significantly larger band gap of *ca.* 3 eV. If the GW calculations are corrected using the Bethe–Salpether equation (BSE), an exciton binding energy of approximately 1 eV is obtained. The experimentally observed band gap is obtained if the GW value is corrected by the exciton binding energy.^{54–56} An alternative approach is the use of the GLLB-SC model, which predicts band gaps of comparable quality compared to those determined at the GW level of theory, but a much lower computational cost.⁵⁷ However, this model also includes the strong exciton binding energy and thus overestimates band gaps for 2D materials.

As in solids, the calculation of the Brillouin zone of the system reflects the ideal crystal, a perfectly planar sheet without deformations or defects. While those calculations are state-of-the-art and accurately yield most results on the electronic structure of these systems, they do not reflect the intrinsic rippling of the monolayers. Ripples can significantly alter the band gap of these systems, for example, ripples in MoS₂ are able to reduce its band gap by \sim 400 meV.¹⁹ Thus, the rippling of 2D systems will unlikely change the character of the systems, but it does have a quantitative effect. As the consideration of rippling is computationally demanding and leads to more difficult analysis of the results due to the absence of an interpretable band structure, it is neglected in most calculations, including those in this article.

Another important issue is the presence of defects in the materials, such as impurities, point defects and grain boundaries.

In 2D materials, defects play a much stronger role than in 3D materials, as there is no third dimension that may act as stabilizing factor, *e.g.* to allow the transmission of a current or to stabilize the structure. Hence, calculations of the perfect crystal only reflect the threshold value of a hypothetical, perfect layer. Defects act as scattering centres and typically reduce the electron transmission. Point defects can strongly influence the electronic properties and even introduce an anisotropy into the system.⁵⁸ The role of the various defects is not yet completely understood and requires more detailed studies both in experiment and in theory.

Thus, the calculation of the band structure yields important information, such as the band gap and its character. Other quantities that are crucial for the prediction of the performance of the materials in electronic applications are the electron transmission, or quantum conductance. The most popular methods to calculate this quantity are the non-equilibrium Green's function (NEGF) method in conjunction with the Landauer-Büttiker formula^{59–61} for small-scale models, and the semi-classical Boltzmann transport equation (BTE), that has been applied for MoS₂ and other 2D materials.^{52,62} The latter one is particularly useful for the prediction of room temperature device performances as it allows the treatment of electron–phonon coupling *via* a perturbation potential.

3. Atomically thin two-dimensional materials

In this section, we discuss graphene and materials that are directly related to this prototype 2D system. Those include isoelectronic hexagonal boron nitride (*h*-BN), 2D materials of the main group IV elements Si and Ge (silicene and germanene), and atomically thin transition metal chalcogenides (TMCs). The most interesting feature about these materials is the significant change in properties compared with their bulk counterparts. Even though some of these systems have not yet

been isolated in free-standing form, they are highly debated in the nanoelectronics community.

3.1. Graphene, silicene and germanene

Even though Boehm coined the term graphene already in 1962,⁶³ the electronic structure of a graphite monolayer has been studied since 1947.⁶⁴ Surprisingly, it was not until 2004 that Geim's group was able to isolate a monolayer graphene sheet.⁵ Afterwards, graphene has been the focus of extensive theoretical and experimental studies. Due to its extraordinary physical properties such as its high carrier mobility and high electrical and thermal conductivity, graphene is considered as a very promising material for nanoelectronics, even being a candidate to replace silicon in future electronic devices. Nevertheless, graphene is a semimetal without band gap, which makes it not suitable for using it as electronic switch (Fig. 3, left). Band gap engineering is thus required to open a band gap in graphene without compromising any of its other properties. The most common techniques and methods reported so far are doping, functionalization, defective or hybrid structures, substrate induced band gap opening, and quantum confinement. To date, a large manifold of potential applications of graphene are under development, and many more have been proposed. These include flexible display screens, electric circuits, and solar cells, as well as medical, chemical, and industrial processes that could be improved by the use of new graphene materials.^{65,66}

Due to the fascinating properties and extensive applications of graphene, scientists started to question whether the other elements in main group IV, *i.e.* Si, Ge, Sn, and Pb, can form stable layered structures. In 2010, Wen *et al.* theoretically explored main group IV structures going from 1D to 2D to 3D.⁶⁷ They found that the graphene layers of Si, Ge, Sn, and Pb essentially collapse to five-coordinated structures with bonds between the layers. The reason is that π -bonding in main group IV, being fundamentally important in all the graphene structures, is only possible for carbon, but not for Si, Ge, Sn, or Pb. Carbon

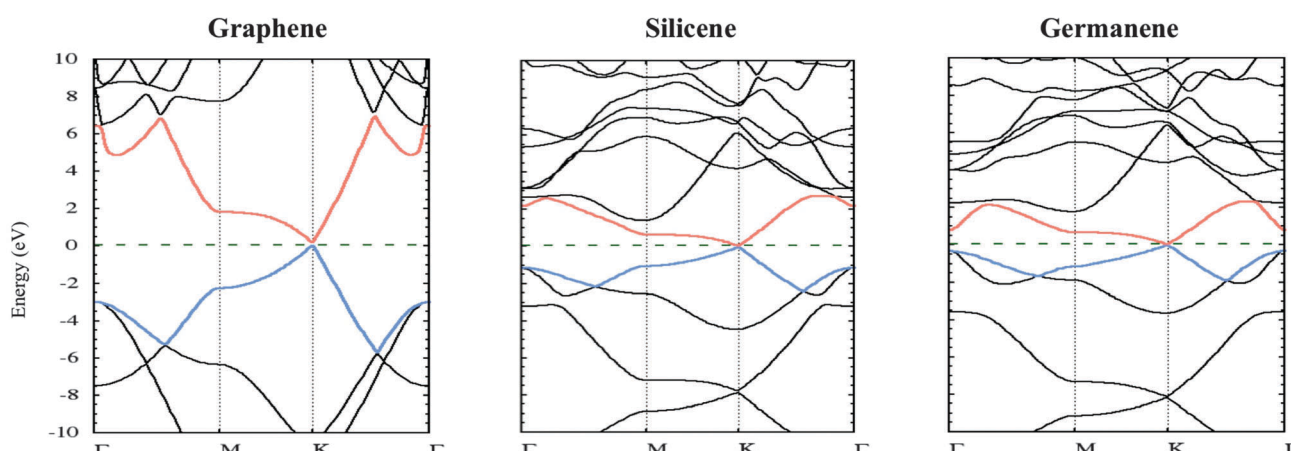


Fig. 3 Band structures of graphene (left), silicene (centre) and germanene (right). Valence and conduction bands are highlighted in blue and red respectively. The Fermi levels (horizontal green dashed lines) have been shifted to 0 eV. All band structures at PBE-D3 level of theory.

effortlessly forms sp^2 hybrid orbitals, the same is not possible for the other elements because of the poor π -type overlap between neighbouring p orbitals at the distance imposed by normal s bonding. Therefore, the graphene-like sheets of Si, Ge, Sn and Pb are very unlikely to have an independent existence. To be consistent with the commonly used nomenclature, silicene is the word to name the silicon analogue of graphene. In the past couple of years, the electronic and structural properties of silicene have been predicted theoretically. Among these studies, Cahangirov *et al.* reported that silicon and germanium can have stable, 2D, slightly corrugated (β -type), honeycomb structures which are more stable than their corresponding planar-layer type counterparts (Fig. 2).⁶⁸ Despite this buckling, the free-standing silicene and germanene structures have enough symmetry to preserve the feature of linearly crossing bands around the Fermi level. This makes electrons of silicene behave as mass-less Dirac Fermions as in graphene (Fig. 3, centre).

Due to its unique bonding behaviour, bulk Si cannot form a layered phase like graphite. However, experiments of surface-assisted epitaxial growth show the presence of nanoribbons and 2D monolayers of silicene on Ag(110)⁶⁹ and Ag(111),^{70–73} respectively. The associated scanning tunnelling microscopy (STM) images revealed hexagons in a honeycomb structure similar to those of graphene. Although free-standing silicene is expected to have a zero band gap, a tiny gap can be opened in epitaxial silicene, due to the symmetry-breaking induced by the interaction with the silver substrate. Vogt *et al.* provided evidence for the successful synthesis of epitaxial silicene sheets on an Ag(111) substrate, by analysing both the structural and electronic properties through the combination of STM and angular-resolved photo-emission spectroscopy (ARPES) in conjunction with DFT calculations.⁷³ Later on, theory predicted that Dirac electrons are absent near the Fermi energy in all stable silicene on Ag(111) structures due to the buckling of the silicene monolayer and hybridization between Si and Ag orbitals.⁷⁴ Recently, silicene has been reported to also grow on ZrB₂ and Ir(111) substrates.^{75,76} Due to the higher mass of Si compared to C, silicene has a stronger SO splitting compared to graphene, it

was predicted to be 1.55 meV.⁷⁷ Another interesting property of silicene is its predicted quantum spin Hall effect in an accessible temperature regime. This property makes silicene particularly interesting for applications as spin Hall effect devices.⁷⁷

Germanene is the germanium analogue of silicene, where the atoms of silicon are replaced by germanium. Up to now, there is no experimental evidence of this system. As in free-standing silicene, it is found that there is no band gap at the Fermi level, indicating metallic properties (Fig. 3, right). The zero band gap observed in germanene originates from the high-buckling distance between the two atomic layers.⁶⁸

Fig. 3 shows the electronic band structure of graphene, silicene and germanene, the latter two in their buckled configurations. All the structures present similar features in the electronic band structure; the bands cross at the Fermi level, located in the Dirac (\mathbf{K}) points of the reciprocal lattice. The linear dispersion around the Dirac points results from the honeycomb structure. Interestingly, this linear dispersion is preserved even when the hybridization of the atoms changes (C is in sp^2 hybridization, while isoelectronic Si and Ge prefer sp^3).

3.2. Boron nitride

Boron nitride exhibits various crystalline polymorphs analogous to carbon, including diamond-like cubic BN, graphite-like hexagonal boron nitride (*h*-BN), onion-like fullerenes, *etc.*⁷⁹ Within these polymorphs, *h*-BN is thermodynamically the most stable allotrope and, due to its 2D nature, has attracted enormous attention. This material is an isoelectronic analogue of graphene, composed of alternating boron and nitrogen atoms in a honeycomb arrangement. sp^2 -bonded *h*-BN shows strong covalent bonds within the plane and weak bonds with van-der-Waals forces between different planes. It is worth mentioning that, in contrast to graphite, bulk *h*-BN favours AA' (eclipsed) stacking.⁸⁰ Regardless of the geometrical similarities, *h*-BN shows strikingly different electronic properties from those of graphene. The former exhibits a direct $\mathbf{K} \rightarrow \mathbf{K}$ band gap between 4.69 eV (PBE) and 7.92 eV (with the GLLB-SC quasi-particle correction) (Table 2), characteristic for

Table 2 Selected properties of atomically thin materials. m_{hh} and m_e stand for the effective mass of the hole, and the electron, respectively. Band gap and effective masses in eV and m_0 (rest mass of electron), respectively⁷⁸

Material	Isolated	Band gap			Effective mass ^a	
		PBE-BJ-D3	GLLB-SC	Transition	m_h	m_{e^-}
Graphene	Yes	0.00 (Dirac point)	0.00 (Dirac point)	\mathbf{K}	—	—
Graphane	Yes	3.56 (direct)	7.00 (direct)	$\Gamma \rightarrow \Gamma$	-0.249	0.983
Fluorographene	Yes	3.29 (direct)	5.16 (direct)	$\Gamma \rightarrow \Gamma$	-0.338	0.466
β -Silicene	Yes	0.00 (Dirac point)	0.00 (Dirac point)	\mathbf{K}	—	—
Silicane	No	2.26 (indirect)	3.56 (indirect)	$\Gamma \rightarrow \mathbf{M}$	-0.128	3.838
Fluorosilicene	No	0.66 (direct)	1.66 (direct)	$\Gamma \rightarrow \Gamma$	-0.128	0.235
β -Germanene	No	0.00 (Dirac point)	0.00 (Dirac point)	\mathbf{K}	—	—
Germanane	Yes	1.16 (direct)	1.84 (direct)	$\Gamma \rightarrow \Gamma$	-0.061	0.063
Fluorogermanene	No	Metallic	0.39 (direct)	$\underline{\Gamma}^b$	-0.017	0.017
<i>h</i> -BN	Yes	4.69 (direct)	7.92 (direct)	$\mathbf{K} \rightarrow \mathbf{K}$	-0.792	1.175
SiC	Yes	2.55 (direct)	3.63 (direct)	$\Gamma \rightarrow \Gamma$	-0.549	0.645

^a From GLLB-SC band structure. Only x direction. ^b In GLLB-SC the transition is $\Gamma \rightarrow \Gamma$.

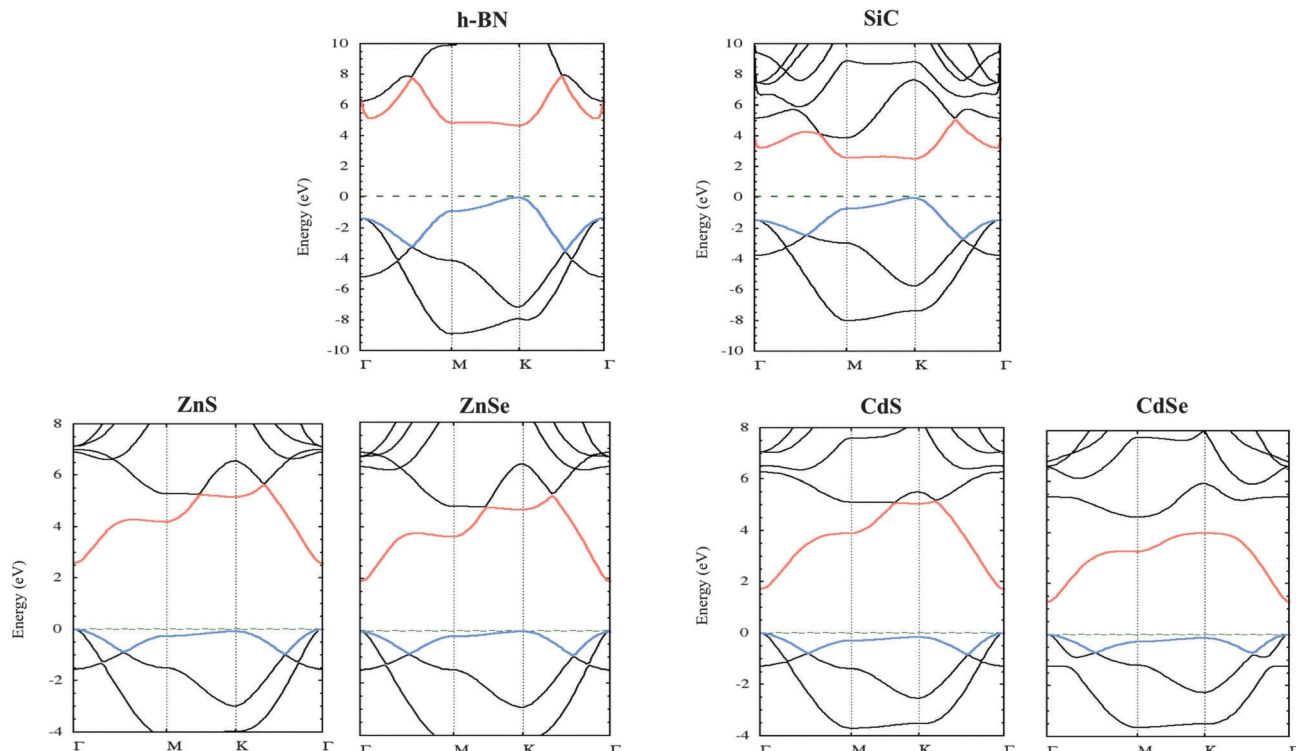


Fig. 4 Band structures of hexagonal boron nitride and silicon carbide (top); atomically thin group XII transition metal chalcogenides (bottom). Valence and conduction bands are highlighted in blue and red respectively. The Fermi levels (horizontal green dashed lines) have been shifted to 0 eV. All band structures at PBE-D3 level of theory.

an insulating white material. The narrowing of the sp^2 π bands (due to the difference in electronegativity) compared with graphene is responsible for the loss of conductivity yielding an insulator instead of a semimetal (Fig. 4, top left).

3.3. Silicon carbide

Naturally, silicon carbide (SiC) occurs in the form of cubic, hexagonal and rhombohedral structures, where Si and C favour sp^3 hybridization. However, a planar structure of SiC with sp^2 -hybridized bonds, thus resembling graphene, was theoretically predicted to have high structural stability.⁸¹ The graphene-like SiC consists of alternating Si and C atoms, where each Si atom has three C atoms as its nearest neighbours and *vice versa*, with a Si-C bond length of 1.79 Å.^{82,83} Due to the Si-C ionicity, the planar SiC system is a semiconductor with a direct K → K band gap of about 2.55 eV (Fig. 4, top right), which increases to 3.63 eV when computed with GLLB-SC as shown in Table 2. Both valence and conduction bands have predominantly Si and C p-orbital character. The upper valence band consists of one π band which arises from the 2p_z and 3p_z orbitals, extending above and below the SiC layer plane, and two σ bands involving the three C 2s, 2p_x, 2p_y and three Si 3s, 3p_x, 3p_y orbitals, which form the Si-C σ bonds.

3.4. Transition metal chalcogenides

Many transition metal chalcogenides (TMCs) present non-layered structures such as zinc blende or wurtzite, while layered TMCs are commonly restricted to metals in groups IV–VI and X. Typical 2D TMCs are transition metal dichalcogenides with a

common formula MX₂, which are not atomically thin. Instead, they are arranged in triatomic layers with a metal sheet sandwiched between two chalcogenide sheets and will be discussed in the next Section. However, during the last years significant advances have been achieved towards the synthesis of atomically thin TMCs. Mono- and multi-layered cadmium sulphides and selenides have been recently synthesized using solvothermal and colloidal techniques.^{84–86} Since the synthesis of these materials was performed in the presence of a surfactant (*e.g.* long chain alkylamines), no free-standing monolayers were isolated. In a different approach, Tusche *et al.*⁸⁷ and Weirum *et al.*⁸⁸ revealed that the deposition of thin layers of zinc oxide on top of a metal substrate leads to the formation of a honeycomb layered structure. These layered materials are less stable than their respective wurtzite bulk ground state phases, however, they could be stabilized by the dispersive interactions between the stacked layers. These advances are highly promising towards the synthesis of free-standing atomically thin group XII TMCs from non-layered materials.

Exfoliated atomically thin TMCs present a honeycomb lattice, however, depending on their composition the sheets are flat (α -type) or slightly corrugated (β -type). Light metal–chalcogenide combinations usually present the former structure (*e.g.* ZnS, ZnSe and CdS), while heavier combinations prefer the latter one (*e.g.* CdSe). DFT calculations on atomically thin zinc and cadmium chalcogenides predict a semiconductor nature with a direct band gap at the Γ point (Fig. 4, bottom). Our band gaps of zinc and cadmium sulphides and selenides obtained at the PBE

Table 3 Selected properties of atomically thin materials transition metal chalcogenides at PBE-BJ-D3 and GLLB-SC levels of theory. m_{lh} , m_{hh} and m_e stand for the effective mass of the light hole, the heavy hole, and the electron, respectively (for explanation of the effective masses, see Scheme 1). Relative stability, band gap and effective masses in meV/formula, eV and m_0 (rest mass of electron), respectively⁷⁸

Material		Rel. stability	Band gap			Effective mass ^a		
			PBE-BJ-D3	GLLB-SC	Transition	m_{lh}	m_{hh}	m_e
ZnS	Flat (α)	0.0	2.58 (direct)	4.50 (direct)	$\Gamma \rightarrow \Gamma$	-0.134	—	0.187
	Corrugated (β)	1.5	2.57 (direct)	4.48 (direct)	$\Gamma \rightarrow \Gamma$	-0.176	-0.178	0.187
ZnSe	Flat (α)	0.0	1.91 (indirect)	3.37 (direct)	$\mathbf{K} \rightarrow \Gamma^b$	-0.107	-0.529	0.126
	Corrugated (β)	3.4	2.01 (direct)	3.48 (direct)	$\Gamma \rightarrow \Gamma$	-0.114	-0.141	0.139
CdS	Flat (α)	0.0	1.72 (direct)	3.23 (direct)	$\Gamma \rightarrow \Gamma$	-0.157	-0.723	0.167
	Corrugated (β)	4.9	1.65 (direct)	3.14 (direct)	$\Gamma \rightarrow \Gamma$	-0.157	-0.751	0.165
CdSe	Flat (α)	9.6	1.20 (indirect)	2.34 (direct)	$\mathbf{K} \rightarrow \Gamma^b$	-0.096	-0.274	0.111
	Corrugated (β)	0.0	1.30 (direct)	2.47 (direct)	$\Gamma \rightarrow \Gamma$	-0.094	-0.141	0.127

^a From GLLB-SC band structure. Only x direction. ^b In GLLB-SC the transition is $\Gamma \rightarrow \Gamma$.

level of theory are in good agreement with previous theoretical studies (Table 3). Besides, recent quasi-particle calculations (GW_0) suggested significantly larger band gaps (4.27 and 3.53 eV for CdS and CdSe, respectively), but they are subject to the exciton binding energy and thus probably overestimate the band gaps.^{89,90} Finally, the GLLB-SC model yields results between PBE and GW_0 values. In all cases, both α and β types are nearly degenerate with an energy difference of a few meV and no overall changes are observed in their band structure.

The experimentally available band gaps for atomically thin ZnS, ZnSe, CdS and CdSe layers are 3.9, 3.5, 2.9 and 2.7 eV, respectively. However, these layers were synthesized in presence of alkylamine surfactants, which induce a major corrugation in the layered structure.⁸⁴ In consequence, these band gaps are not directly comparable with the calculated ones where the surfactants are absent and corrugation is nonexistent or minimal.

In these materials, two bands converge at the valence band maximum (the Γ -point). The flatter band is known as heavy-hole band, while the steeper one is the light-hole band (Scheme 1). The heavy and light hole effective masses (m_{lh} and m_{hh} , respectively) of a semiconductor is obtained by fitting the area in the k space around these bands maximum to a parabola. The effective mass reflects the inverse of the band curvature, in consequence the lower the effective mass the larger the band curvature is.

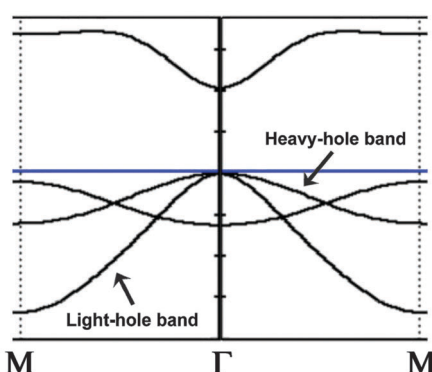
Analogously, the electron effective mass (m_e) is obtained by fitting the minimum of the conduction band. Effective masses are related to charge carrier mobilities and thus, consequently, to the electric and thermal conductivities of the materials. The effective masses for atomically thin TMCs are presented in Table 3.

4. Ultrathin 2D materials

In this section, we discuss 2D materials that are more than one atom thick (ultrathin materials). We limit our study to three families of ultrathin 2D materials: hydrogenated and fluorinated graphene, silicene and germanene derivatives; rare earth, semimetal and transition metal chalcogenides; and rare earth and transition metal halides. Some of the presented systems have not yet been isolated in their bulk and/or free-standing form, however, the theoretical prediction of their properties is the vanguard for the experimental growth and isolation of the most promising materials.

4.1. Graphane, silicane and germanane

Chemical functionalization, especially hydrogenation and fluorination, are being used to tailor the electronic properties of graphene-like materials. Here we describe briefly the latest studies on these saturated structures. In 2013, Bianco *et al.* reported the synthesis of stable, single-layered germanane using topotactic deintercalation. This involves a structural change to a crystalline solid and the final lattice is related to the original material by one or more crystallographically equivalent orientations.⁹¹ A large crystal of $\beta\text{-CaGe}_2$ was converted into a layered GeH when placed in aqueous HCl at 40 °C. $\beta\text{-CaGe}_2$ has alternating planes of covalently bonded germanium atom layers separated by ionically bonded interstitial calcium. The bonding type in germanane appears to have mixed sp^2 and sp^3 hybridization. Ultrathin germanane has a remarkable resistance to oxidative degradation and has been found to be stable over five months in air. Germanane, unlike silicane, does not require a substrate to be stable. The atomic structure of germanane is slightly corrugated rather than flat like graphane or graphene (Fig. 2). Calculations do not show the existence of a Dirac cone, but germanane still has a surprisingly



Scheme 1 Heavy- and light-hole bands for ZnS. The Fermi level (blue line) has been shifted to 0 eV.

high electron mobility, which is much higher than that of its bulk material. A theoretical analysis showed that germanane has a direct band gap of 1.53 eV, making it a potential material for solar cells.⁹² Contrary to graphane, the hydrogenation in germanane is not a reversible process. It becomes an amorphous material above 75 °C.

4.2. Fluorographene, fluorosilicene and fluorogermanene

Fluorographene is the fluorinated derivative of graphene, namely, it is a 2D carbon monolayer of sp^3 hybridized carbons, with each carbon atom bound to one fluorine atom. Similar to other fluorocarbons, fluorographene is highly insulating and has a high thermal and chemical stability. However, it can be transformed back into graphene by a reaction with potassium iodide under high temperature.

Fluorographenes are expected to present similar structural and electronic characteristics as graphene. However, since fluorine has a much larger electronegativity than hydrogen, the charge transfer between graphene and F atoms in fluorographene is distinctive from that in graphene. The single-layer fluorographene exhibits a wide band gap semiconducting behaviour with an optical gap of *ca.* 3 eV; which is in good agreement with the recent experimentally measured one of around 3.8 eV.⁹³ Nevertheless, first principle calculations show again that the estimation of the band gap can be a challenging

task, as GGA provides a band gap of 3.29 eV, hybrid (HSE06) 4.9 eV, while many-electron approaches based on GW approximation give a band gap of 8.1 eV (twice as large).⁹⁴ Therefore, it is necessary to include the exciton binding energy to obtain the correct band gap value. Band structures of fluorinated and hydrogenated graphene and its analogues are given in Fig. 5.

Fluorinated silicene was theoretically studied by Ding *et al.*,⁹⁵ who reported that it has a direct band gap which values can be tuned by strain in the lattice. The values of the formation energies for these structures are negative, indicating that the hydrogenation/fluorination of silicene is an exothermic reaction and the corresponding H-/F-silicene is stable.

4.3. Transition metal chalcogenides and semimetal chalcogenides

Transition metal chalcogenides (TMCs) form a family of materials with a general formula M_nX_m , where M is a transition metal and X is always a chalcogenide element. Layered TMCs have been reported with elements of group IV (Ti, Zr and Hf), group VI (Mo and W), group V (Pd and Pt) as well as with Ta, Re and Nb.⁹⁶ These materials always present a MX_2 stoichiometry and are composed of 2D sheets stacked on top of one another. Each sheet is three atoms thick, with a metal atom in the middle that is strongly bonded to chalcogenide atoms located above and below (Fig. 2). The intralayer metal–chalcogen bond is

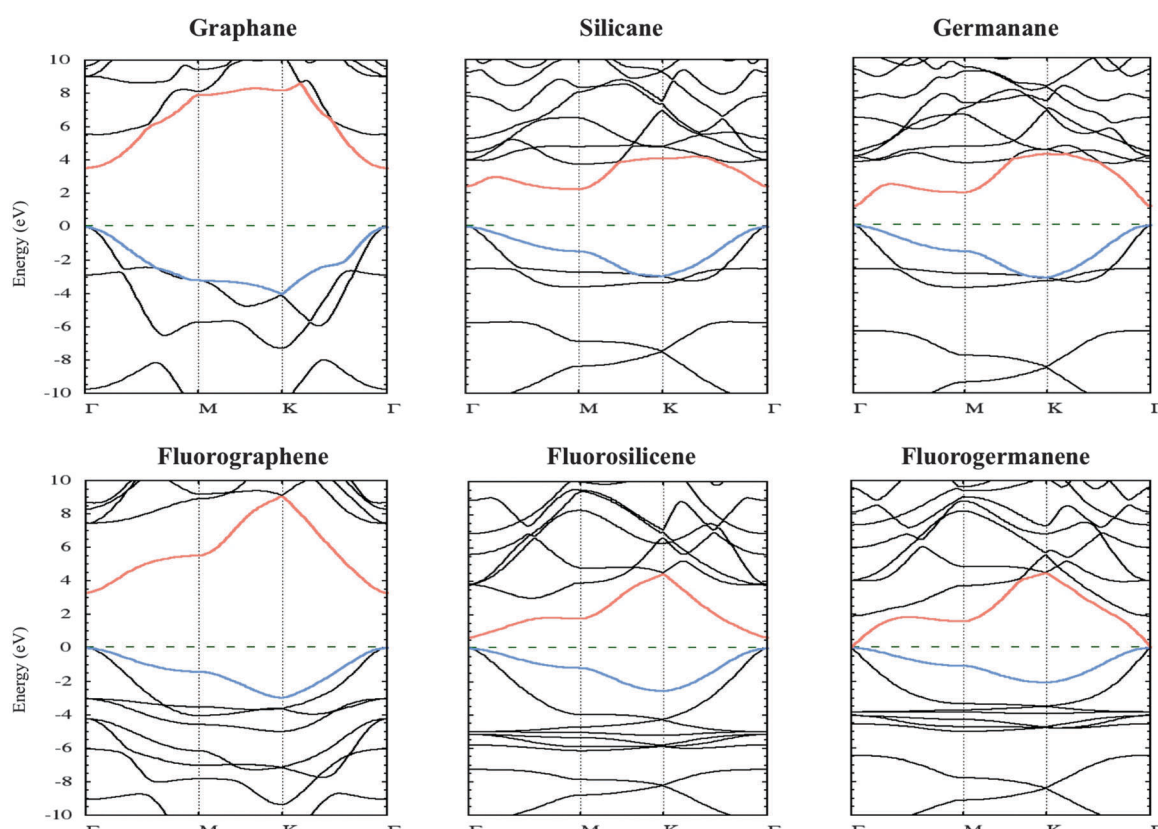


Fig. 5 Band structures of hydrogenated (top) and fluorinated (bottom) derivatives of graphene (left), silicene (centre) and germanene (right). Valence and conduction bands are highlighted in blue and red respectively. The Fermi levels (horizontal green dashed lines) have been shifted to 0 eV. All band structures at PBE-D3 level of theory.

predominantly covalent in nature, while the sheets are held together by weak interlayer interactions (London dispersion). This facilitates the shearing of TMC layers, which has led to the initial applications of these materials as high performance lubricants.⁹⁷ Layered TMCs only occur in two polytypes, in both the metal centre either has a trigonal prismatic (H = hexagonal or rhombohedral) or octahedral (T = trigonal prismatic or octahedral) environment.

Recently, TMCs have emerged as a graphene alternative, as they display unique chemical and physical properties that are absent or difficult to obtain in other 2D materials. For example, in graphene, complex band gap engineering is required towards its applications as transistors. Various TMC representatives, however, are inherent semiconductors.⁹⁸ Furthermore, TMCs present a wide variety of electronic properties including metals, semimetals, insulators and semiconductors with direct and indirect band gaps and a range of electron and hole mobilities depending on their composition. Consequently, these materials have a variety of highly desirable characteristics affecting charge transport, magnetism, the intercalation of ions and small molecules, and their catalytic and optical properties.

The most prominent TMCs are MoS₂, WS₂, MoSe₂ and WSe₂ (sometimes referred to collectively as MoWSeS) that have been widely studied for applications in electronics since they are semiconductors. The band gaps of these materials can be "easily" tuned by stacking confinement and strong electric fields, as recently shown by Zibouche *et al.*⁹⁹ For example, bulk MoS₂ has an indirect band gap of 0.9 eV, while at the monolayer limit it switches to a direct band gap of 1.8 eV.²² The transition from indirect to direct bandgap has a huge implication when studying photoluminescence as the latter increases when decreasing the layer thickness.^{100–102} Other features that make MoWSeS interesting for applications in nanoelectronics are chemical stability, the absence of dangling bonds (except at the sheet edges and corners), and thermal stability up to ≈ 1100 °C. Radisavljevic *et al.* have recently demonstrated that single-layer MoS₂ can be used to fabricate transistors with high electron mobility and high current on/off ratios.¹⁴ As similar manufacturing principles as in silicon semiconductor electronics are feasible, including gating and contacting, complex devices suitable for building integrated circuits are possible. Indeed, logic operations and integrated circuits and nonvolatile memory cells based on single-layer MoS₂ and MoS₂/graphene have been recently demonstrated.^{14,92,103–108} Moreover, the high stiffness and breaking strength of MoWSeS materials has shown their compatibility for the use in flexible electronics.^{19,109–112} These studies are part of the vanguard of a rapidly emerging field, 2D materials beyond graphene. And, while devices based on MoWSeS materials are blooming,^{104,113} basic research on other layered TMCs is still in early stages.

Two examples of semiconducting TMCs beyond MoWSeS are those based on the early transition metals (*e.g.* TiS₂, ZrS₂, HfS₂...) and the noble metals (PdS₂, PtS₂...). Members of the former class have recently been explored as nanodisises due to a large anisotropy between their in-plane and out-of-plane growth.^{114–116} In addition,

Jeong *et al.* studied the chemical reactivity of the edge and basal planes and their use in hybrid materials (*e.g.* TiS₂–TiO₂) with enhanced solar energy uptake and facilitated electron-transfer properties.¹¹⁷ The noble TMC class, by contrast, has been known for almost a century and was theoretically studied recently, but their exfoliation and application as 2D materials has yet to be pursued.^{41,118}

The electronic structure of bulk layered TMCs has been previously studied by means of *ab initio* calculations using the plane wave approach as well as by employing local basis functions. Among them, we selected zirconium, niobium, molybdenum, and palladium disulphides as representative materials for both T and H polytypes. The metals in these materials have formally an oxidation state of IV, leading to Zr⁴⁺(d⁰), Nb⁴⁺(d¹) Mo⁴⁺(d²), and Pd⁴⁺(d⁶) metal centres. The crystal field theory predicts a small d orbital splitting for transition metals in presence of chalcogenide ligands. This allows a qualitative prediction of the electronic nature of these materials without quantum mechanical calculations. However, the d orbital splitting for H and T polytypes differs and is well established. For the former, this splitting derives in three orbital groups of increasing energy (d_{z2}; d_{xy} and d_{x²-y²}; d_{xz} and d_{yz}), while on the latter a traditional octahedral field orbital splitting is observed (d_{xy}, d_{xz} and d_{yz}; d_{z2} and d_{x²-y²}). The band structures of the representative materials are shown in Fig. 6. Trigonal and hexagonal zirconium disulphides present always a semiconductor band structure with band gaps of *ca.* 1 eV, however, the trigonal polytype is the energetically most favourable one. Molybdenum disulphide is a metal in T polytype, but a direct band gap semiconductor (1.82 eV) in the H form, which is the most stable and common one. On the contrary, niobium disulphides are always metallic, independently on the polytype due to the unpaired electron in the metal centre. Finally, the palladium disulphide trigonal polytype is an indirect band gap semiconductor with a $\Gamma \rightarrow \frac{1}{2}\mathbf{M}$ transition, while the hexagonal polytype is a metal.

Semimetal chalcogenides (SMCs) are a family of layered materials similar to TMCs, but including a semimetal instead of transition metals. Their most common stoichiometry is M₂X₂ in X–M–M–X tetraatomic thick layers (Fig. 2). Gallium and indium sulphides and selenides are among the most prominent materials in this family. They are predicted to be semiconductors with indirect $\frac{1}{2}\mathbf{M}$ to Γ band gaps of 2.57, 2.05, 2.09, and 1.70 eV for GaS, GaSe, InS, and InSe, respectively, within the PBE level of theory (Fig. 7). Recent theoretical studies pointed out that possible direct and indirect transitions are only slightly different in energy. This difference is small enough to allow the switching between direct and indirect semiconductors for GaS and GaSe by thermal energy.¹¹⁹ Furthermore, the band gaps of SMC monolayers can be tuned by mechanical deformation, making these materials potential candidates for novel nanodevices. The GLLB-SC model predicts significantly larger band gaps, which lay in the insulator range in many cases, however, due to the excitonic effects, the GLLB-SC band gaps are overestimated (Table 4).

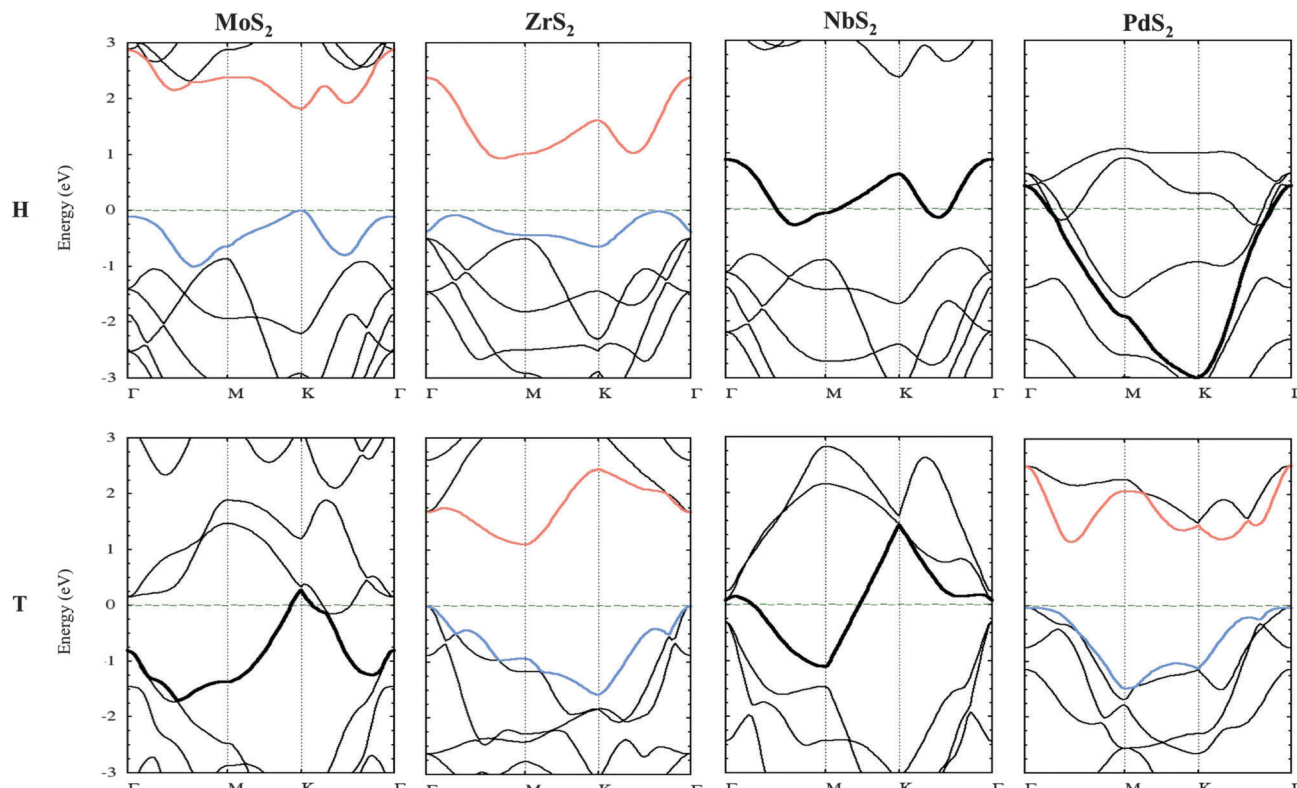


Fig. 6 Band structures of H (top) and T (centre) polytypes of MoS_2 , ZrS_2 , NbS_2 and PdS_2 transition metal chalcogenides (left to right respectively). Valence and conduction bands are highlighted in blue and red respectively. The Fermi levels (horizontal green dashed lines) have been shifted to 0 eV. All band structures at PBE-D3 level of theory.

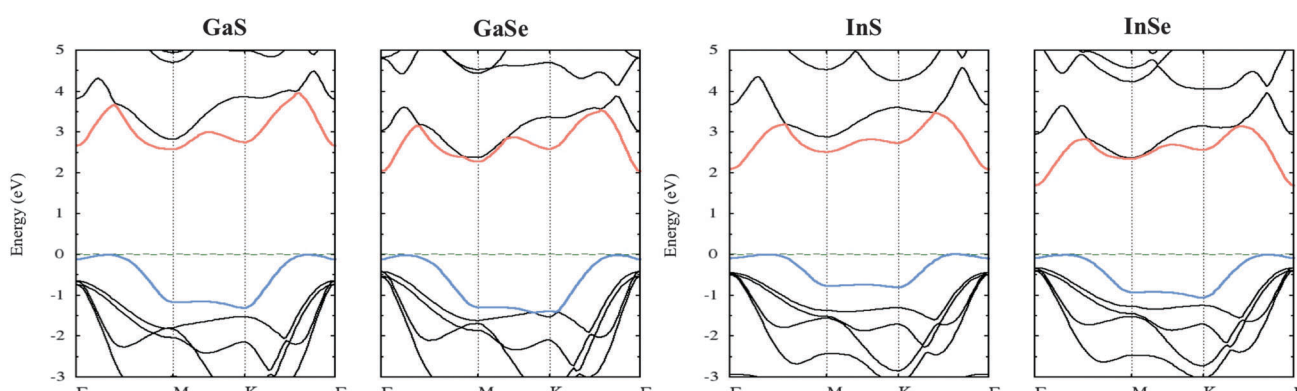


Fig. 7 Band structures of gallium (left) and indium (right) chalcogenides. Valence and conduction bands are highlighted in blue and red respectively. The Fermi levels (horizontal green dashed lines) have been shifted to 0 eV. All band structures at PBE-D3 level of theory.

4.4. Transition metal halides

Transition metal halides (TMHs) encompass a family of materials with the general formula M_nY_m , where M is a transition metal and X is always a halogen element. Only few 3D layered TMH materials have been observed experimentally, such as cadmium, vanadium and molybdenum halides.¹²⁰ However, their exfoliation down to the monolayer still remains unachieved. Two main stoichiometries (MY_2 and MY_3) have been observed in experimental TMHs, with the metal centre in a trigonal prismatic (octahedral) environment

in both cases. Analogously to TMC materials, the 2D TMH sheets are triatomic (halide–metal–halide) and stacked on top of each other (Fig. 2). The interlayer interaction is also mainly dominated by weak interlayer interactions (London dispersion).

Initially, we want to focus on the electronic structure of TMH monolayers with MY_2 stoichiometry from which we selected calcium, manganese, iron and nickel chlorides and bromides as TMH representative materials. This derives formally in $\text{Ca}^{2+}(\text{d}^0)$, $\text{Mn}^{2+}(\text{d}^5)$, $\text{Fe}^{2+}(\text{d}^6)$ and $\text{Ni}^{2+}(\text{d}^8)$ metal centres. The crystal field theory predicts a small d orbital splitting for transition metals in

Table 4 Selected properties of transition metal chalcogenides and semimetal chalcogenides at PBE-BJ-D3 and GLLB-SC levels of theory. m_{lh} , m_{hh} and m_e stand for the effective mass of the light hole, the heavy hole, and the electron, respectively. Band gap, spin orbit splitting and effective masses in eV, meV and m_0 (rest mass of electron), respectively⁷⁸

Material	Band gap					Effective mass ^a		
	PBE-BJ-D3 (scalar)	PBE-BJ-D3 (SO)	SO splitting	GLLB-SC	Transition	m_{lh}	m_{hh}	m_e
ZrS_2	T 1.10 (indirect)	1.06 (indirect)	80	2.30 (indirect)	$\Gamma \rightarrow \mathbf{M}$	-0.218	-0.221	1.869
	H 0.92 (indirect)	0.90 (indirect)	20	2.03 (indirect)	b	—	-0.726	13.881
MoS_2	T Metallic	Metallic	—	Metallic	—	—	—	—
	H 1.82 (direct)	1.74 (direct)	150	2.51 (direct)	$\mathbf{K} \rightarrow \mathbf{K}$	—	-0.557	0.463
NbS_2	T Metallic	Metallic	—	Metallic	—	—	—	—
	H Metallic	Metallic	—	Metallic	—	—	—	—
PdS_2	T 1.17 (indirect)	1.15 (indirect)	80	1.73 (indirect)	$\Gamma \rightarrow \frac{1}{2}\mathbf{M}$	-0.725	-0.638	0.407
	H Metallic	Metallic	—	Metallic	—	—	—	—
GaS	— 2.57 (indirect)	2.56 (indirect)	—	4.12 (indirect)	$\frac{1}{2}\mathbf{M} \rightarrow \Gamma$	—	-2.755	2.020
GaSe	— 2.05 (indirect)	2.02 (indirect)	—	3.38 (indirect)	$\frac{1}{2}\mathbf{M} \rightarrow \Gamma$	—	-2.007	0.173
InS	— 2.09 (indirect)	2.09 (indirect)	—	3.58 (indirect)	$\frac{1}{2}\mathbf{M} \rightarrow \Gamma$	—	-3.758	0.313
InSe	— 1.70 (indirect)	1.66 (indirect)	—	2.93 (indirect)	$\frac{1}{2}\mathbf{M} \rightarrow \Gamma$	—	-3.228	0.213

^a From GLLB-SC band structure. Only x direction. ^b Check Fig. 6. Computational details are given in Section 7.

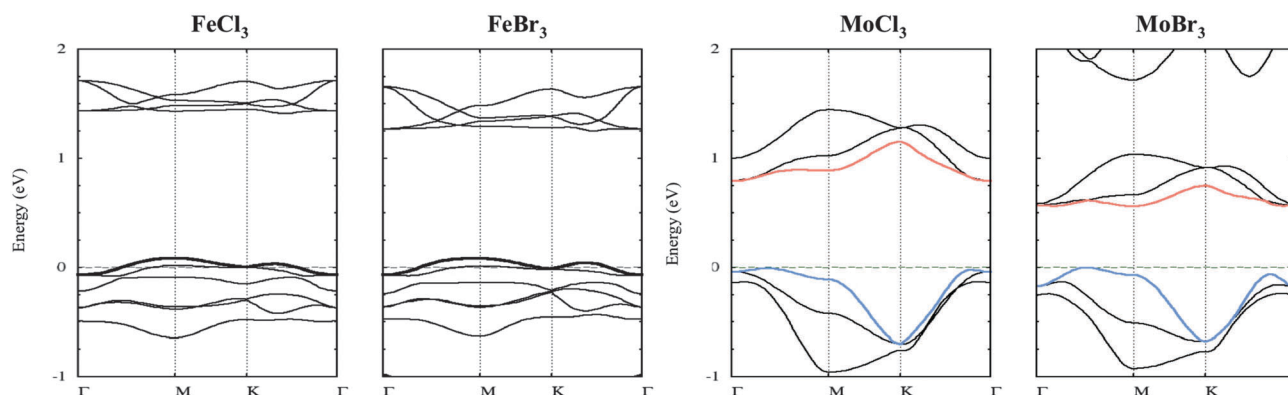


Fig. 8 Band structures of iron (left) and molybdenum (right) transition metal chlorides and bromides (MY_3 stoichiometry). Valence and conduction bands are highlighted in blue and red respectively. The Fermi levels (horizontal green dashed lines) have been shifted to 0 eV. All band structures at PBE-D3 level of theory.

presence of ligands at the beginning of the spectrochemical series (such as halogens). This makes it difficult to predict the electronic nature of these materials with the exception of calcium halides, which are expected to be insulators due to the completely empty 4s and 3d bands. DFT calculations on TMHs predict wide varieties of electronic structures and confirm the small d orbital splitting (e.g. Mn in manganese halides is predicted to be high spin; 5 electrons in 5d orbitals) (see page S54, ESI†). Manganese halides are high spin small band gap semiconductors (0.38 and 0.18 eV for MnCl_2 and MnBr_2 , respectively); iron halides are always metallic due to the partial filling of the metal d orbitals (6 electrons in 5 orbitals); finally nickel halides are high spin semiconductors with band gaps of 1.06 and 0.64 eV, respectively, at the PBE level of theory. Furthermore, the band gap in semiconducting TMH materials decreases when going down in the halogen group, in agreement with the smaller crystal field splitting ($\text{I} < \text{Br} < \text{Cl} < \text{F}$) predicted in the spectrochemical series.¹²¹ Thus, these trends confirm the d nature of the frontier bands above and under the Fermi energy. Analogously with TMC monolayers, calculations with GLLB-SC model largely overestimate TMH band gaps.

Finally we present TMH monolayers with MY_3 stoichiometry. The unit cells of these materials are similar to the MY_2 ones, where one of every three metal centres has been removed. In consequence, these materials present a slightly larger d orbital splitting and their metal centres are in oxidation state III. On one hand, iron halides are metallic since the metal electrons (5) are localized in the three t_{2g} orbitals (d_{xy} , d_{xz} and d_{yz}), while the e_g orbitals lay higher in energy. On the other hand, their molybdenum analogues are semiconductors with partially filled t_{2g} orbitals that lead to band gaps of 0.80 and 0.56 eV in MoCl_3 and MoBr_3 , respectively, at PBE level of theory (Fig. 8 and Table 5).

5. Synthetic 2D organic frameworks

5.1. Layered covalent organic frameworks

Covalent organic frameworks (COFs) are crystalline porous materials formed from the covalent bonding of light elements (H, B, C, N and O). COFs have low mass densities, possess high thermal stabilities, and provide permanent porosity. COFs can

Table 5 Selected properties of MY_2 and MY_3 transition metal halides at PBE-BJ-D3 level of theory. m_{lh} , m_{hh} and m_e stand for the effective mass of the light hole, the heavy hole, and the electron, respectively. Band gap and effective masses in eV and m_0 (rest mass of electron), respectively⁷⁸

Material	Band gap			Effective mass ^a		
	PBE-BJ-D3	GLLB-SC	Transition	m_{lh}	m_{hh}	m_e
CaCl_2	5.97 (indirect)	9.92 (indirect)	$\Gamma \rightarrow \mathbf{M}$	—	-2.156	1.698
CaBr_2	5.13 (indirect)	10.32 (indirect)	$\Gamma \rightarrow \mathbf{M}$	-0.621	-2.224	0.384
MnCl_2	0.37 (direct)	— ^b	$\mathbf{M} \rightarrow \mathbf{M}^c$	— ^{c,d}	-1.079 ^{c,d}	2.582 ^{c,d}
MnBr_2	0.18 (indirect)	— ^b	$\Gamma \rightarrow \mathbf{M}^c$	-0.314	-0.326 ^{c,d}	2.862 ^{c,d}
FeCl_2	Metallic	Metallic	—	—	—	—
FeBr_2	Metallic	Metallic	—	—	—	—
NiCl_2	1.06 (indirect)	— ^b	$\Gamma \rightarrow \mathbf{M}^c$	-0.490 ^{c,d}	-0.549 ^{c,d}	2.447 ^{c,d}
NiBr_2	0.64 (indirect)	— ^b	$\Gamma \rightarrow \mathbf{M}^c$	-0.286 ^{c,d}	-1.154 ^{c,d}	1.988 ^{c,d}
FeCl_3	Metallic	Metallic	—	—	—	—
FeBr_3	Metallic	Metallic	—	—	—	—
MoCl_3	0.80 (indirect)	1.20 (indirect)	$\frac{1}{2}\mathbf{M} \rightarrow \Gamma$	-1.748	-8.239	3.291
MoBr_3	0.56 (indirect)	0.87 (indirect)	$\frac{1}{2}\mathbf{M} \rightarrow \Gamma$	-0.382	-42.664	3.591

^a From GLLB-SC band structure. Only x direction. ^b GLLB-SC not implemented for unrestricted calculations. ^c From PBE-BJ-D3 band structure.

^d Holes spin up, electrons spin down.

be known to crystallize in either 2D or 3D forms. If connectors and linkers are planar, layered COFs can be obtained (most of the boronic-acid-derived bulk COFs). Indeed, the first COFs that have been reported are layered materials. Their structures have been denoted by the Yaghi group as COF-*n*, *n* being an integer labelling the material in the historical order of their synthesis.²⁵

More recently, Banerjee and co-workers have extended the range of connectors and linkers *e.g.* by using boroxine and 1,3,5-triformylphloroglucinol.^{122–126} A large number of phenyl-based molecules have been used as linkers such as phenyl, *meta*-terphenyl and hexadecahydrophyrone, leading to a wide variety of 2D COFs (Fig. 9). As another alternative, Xu *et al.* have

used Schiff-base coupling on solid surfaces. They mixed different linkers, principally benzene-1,3,5-tricarbalddehyde, with diamine in octanoic acid and let them polymerize on a surface while heating moderately. Using this approach, Xu *et al.* prepared four well-ordered honeycomb Schiff-base surface COFs on a HOPG surface.¹²⁷ The lone pair electrons of nitrogen make the Schiff-base group a good ligand for coordination, thus these Schiff-base surface COFs can be potentially used in the field of chemical sensing and catalysis. 2D COFs are predicted to be stable in organic media, but exfoliation techniques to obtain single layers are still a hot topic. First Covalent Organic Nanosheets (CONs), exfoliated by micromechanical means, have been reported recently by the Banerjee group.¹²³

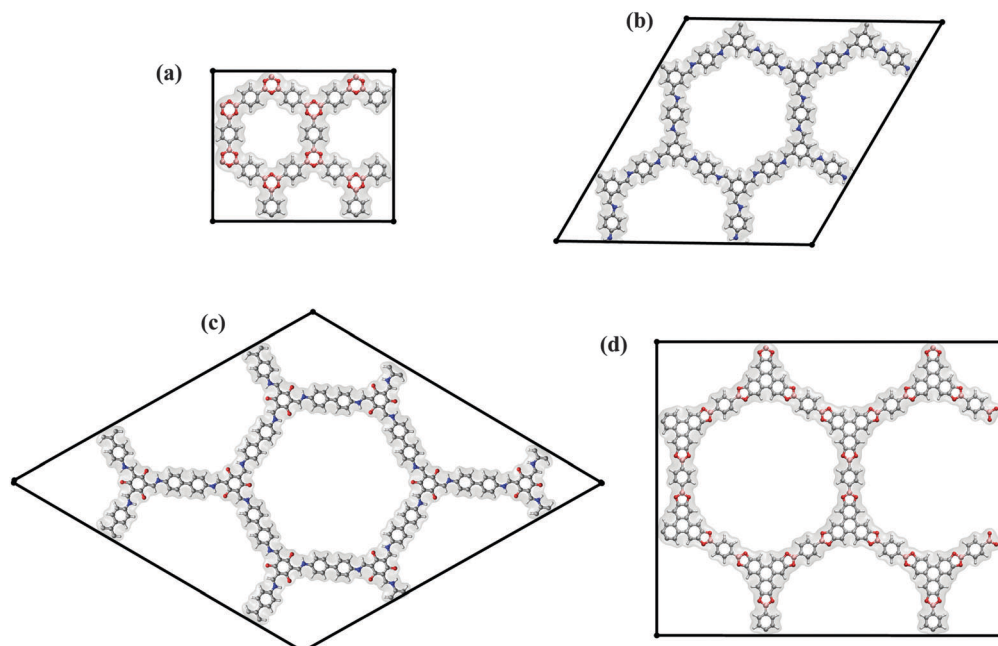


Fig. 9 Selected examples of layered covalent organic frameworks (COFs): COF-1 (a), COF reported by Xu and co-workers (b), COF incorporating in-plane hydrogen bridges reported by Banerjee and co-workers. (c) COF-5 (d). Colour code: boron in pink, oxygen in red, nitrogen in blue, carbon in grey and hydrogen in white. Unit cell is depicted in black.

The electronic structure of 2D COFs has been predicted to be insulating or semiconducting. The band gap is typically very similar to the smallest HOMO–LUMO gap of the constituting molecules, confirming the concept of reticular chemistry.¹²⁸ For example, single layer phenyl/boroxine, *meta*-terphenyl/boroxine, hexadecahydronaphthalene/boroxine, biphenyl/boroxine and hexadecahydronaphthalene COFs have gaps larger than 2 eV, respectively, at PBE level of theory and using the Γ point approximation. This restricts their application in nanoelectronics. However, their porous nature opens new possibilities towards the development of 2D nanoporous organic membranes (nanosieves). The membrane selectivity could be tuned with the pore size as well as with the proper linker functionalization.

6. Conclusions and perspectives

The discovery of 2D materials has started a new era of materials science. New materials, atomically thin and mechanically, thermally and electronically stable, with a large variety of electronic properties are available and they can be assembled in ultrathin flexible devices. The manufacturing of new devices requires the detailed understanding of the properties of 2D materials, which is supported by the electronic properties presented in this work. Band gaps and effective electron and hole masses allow the estimation of charge and spin mobilities for basic device simulations. The band structures, given in the ESI,[†] allow the parameterization of tight-binding models that are useful for more elaborate electron transport calculations and device simulations. Our results show that all classes of materials that are known from the 3D world have counterparts in 2D. We find metals and insulators, semiconductors with a large variety of band gaps and with different band features. In addition, 2D materials exhibit properties that are unknown from the bulk, for example massless Dirac electrons.

DFT works very well for predicting the structure of 2D materials. It should be reminded that – if interlayer interactions are investigated – presently available DFT functionals need to be augmented by a scheme that corrects for the missing London dispersion interactions.

DFT yields excellent band structures, however, the position of the conduction bands, and hence the band gaps, tend to be underestimated. The quenched Coulomb screening in 2D materials causes strong exciton binding energies of ~ 1 eV. This energy is included in the electronic band gaps predicted by quasiparticle theories such as the GW approximation or the GLLB-SC model. In some cases, *e.g.* in the MoWSeS TMCs, this leads to an error cancellation for DFT functionals that perform very well for these systems.

In 2D materials, the ultimate frontier of miniaturization has been reached – at least in one dimension. The calculations of properties of 2D infinite layers are state-of-the-art. However, calculations beyond that limit are still demanding. Besides the obvious challenges such as the inclusion of structural and stoichiometric defects and doping, a remaining issue is lateral quantum confinement, where electronic and optical properties depend on the lateral size of the 2D structures.^{114,129} Another

important problem is the interaction of the 2D materials with substrates and other factors present in their environment. The enormous progress in the field of 2D materials suggests that many of those challenges will be tackled in the not too distant future. In this vein it is interesting to note that special issues on 2D materials beyond graphene are planned for 2014, one in *Accounts of Chemical Research* and another one in *Chemical Society Reviews*.

7. Computational details

All DFT calculations were performed using the Amsterdam Density Functional (ADF2013-BAND) package.^{29–31} We used the local VWN exchange–correlation potential with nonlocal Perdew–Burke–Ernzerhof exchange–correlation correction and empirical D3 treatment of London dispersion interactions (PBE–BJ–D3).^{50,51,130} A triple- ζ plus two-polarization function basis set was used for all atoms. Relativistic corrections were introduced by scalar relativistic zeroth order regular approximation (ZORA).^{42–46} Both \mathbf{k} -space and accuracy were set to 5. All band structures have been evaluated on the PBE–BJ–D3 optimized structures including spin–orbit corrections. Additional calculations using the M06-L meta-GGA exchange–correlation functional and the GLLB-SC model^{57,131} have been performed. The former ones are given in the ESI,[†] while the latter ones are included in the tables of the main text.

8. The atlas of 2D materials

For all the materials discussed in this article and additional ones, Cartesian coordinates, electronic band structures, band gaps and effective masses of electrons and holes are available as part of the ESI.[†]

8.1. Atomically thin 2D materials

Graphene, graphane, fluorographene, chlorographene, silicene, silicane, fluorosilicene, germanene, germanane, fluorogermanene, chlorogermanene, silicon carbide, boron nitride, α -ZnO, α -ZnS, α -ZnSe, α -ZnTe, α -CdO, α -CdS, α -CdSe, α -CdTe, β -ZnS, β -ZnSe, β -ZnTe, β -CdO, β -CdS, β -CdSe and β -CdTe.

8.2. Ultrathin 2D materials

GaS, GaSe, InS, InSe, HfS₂, HfSe₂, HfTe₂, MoS₂, MoSe₂, MoTe₂, NbS₂, NbSe₂, NbTe₂, NiS₂, NiSe₂, NiTe₂, PdS₂, PdSe₂, PdTe₂, PtS₂, PtSe₂, PtTe₂, ReS₂, ReSe₂, ReTe₂, TaS₂, TaSe₂, TaTe₂, TiS₂, TiSe₂, TiTe₂, WS₂, WSe₂, WTe₂, ZrS₂, ZrSe₂, ZrTe₂, CoCl₂, CoBr₂, FeCl₂, FeBr₂, FeI₂, HfCl₂, HfBr₂, HfI₂, MnCl₂, MnBr₂, MnI₂, MoCl₂, MoBr₂, MoI₂, NbCl₂, NbBr₂, NbI₂, NiCl₂, NiBr₂, TaCl₂, TaBr₂, TaI₂, TiCl₂, TiBr₂, TiI₂, VCl₂, VBr₂, VI₂, WCl₂, WBr₂, WI₂, ZrCl₂, ZrBr₂, ZrI₂, AsCl₃, CrCl₃, CrBr₃, CrI₃, FeCl₃, FeBr₃, MoCl₃, MoBr₃, SbCl₃, ScCl₃, ScBr₃, TiCl₃, TiBr₃, VCl₃, VBr₃, YCl₃ and ZrCl₃.

Acknowledgements

This work was supported by the German Research Council (Deutsche Forschungsgemeinschaft, HE 3543/18-1), The European Commission (FP7-PEOPLE-2009-IAPP QUASINANO, GA 251149 and

FP7-PEOPLE-2012-ITN MoWSeS, GA 317451), The Office of Naval Research Global (N62909-13-1-N222). We thank Dr Agnieszka Kuc and Mr Mahdi Ghorbani-Asl for critically reading and commenting the manuscript; and Mr Wenqing Liu for the help with the plane wave calculations.

Notes and references

- 1 L. D. Landau and E. M. Lifshitz, *Statistical Physics, Part I & II*, Pergamon Press, Oxford, 1980.
- 2 R. E. Peierls, *Ann. Inst. Henri Poincare*, 1935, **5**, 177–222.
- 3 R. E. Peierls, *Helv. Phys. Acta*, 1934, **7**, 81–83.
- 4 N. D. Mermin, *Phys. Rev.*, 1968, **176**, 250–254.
- 5 K. S. Novoselov, A. K. Geim, S. V. Morozov, D. Jiang, Y. Zhang, S. V. Dubonos, I. V. Grigorieva and A. A. Firsov, *Science*, 2004, **306**, 666–669.
- 6 C. N. R. Rao, A. K. Sood, K. S. Subrahmanyam and A. Govindaraj, *Angew. Chem., Int. Ed.*, 2009, **48**, 7752–7777.
- 7 V. Nicolosi, M. Chhowalla, M. G. Kanatzidis, M. S. Strano and J. N. Coleman, *Science*, 2013, **340**, 1226419.
- 8 J. N. Coleman, M. Lotya, A. O'Neill, S. D. Bergin, P. J. King, U. Khan, K. Young, A. Gaucher, S. De, R. J. Smith, I. V. Shvets, S. K. Arora, G. Stanton, H.-Y. Kim, K. Lee, G. T. Kim, G. S. Duesberg, T. Hallam, J. J. Boland, J. J. Wang, J. F. Donegan, J. C. Grunlan, G. Moriarty, A. Shmeliov, R. J. Nicholls, J. M. Perkins, E. M. Grieveson, K. Theuwissen, D. W. McComb, P. D. Nellist and V. Nicolosi, *Science*, 2011, **331**, 568–571.
- 9 K. Ramasamy, H. Sims, W. H. Butler and A. Gupta, *J. Am. Chem. Soc.*, 2014, **136**, 1587–1598.
- 10 R. F. Frindt and A. D. Yoffe, *Proc. R. Soc. London, Ser. A*, 1963, **273**, 69–83.
- 11 L. F. Mattheiss, *Phys. Rev. Lett.*, 1973, **30**, 784–787.
- 12 L. F. Mattheiss, *Phys. Rev. B: Solid State*, 1973, **8**, 3719–3740.
- 13 P. Joensen, R. F. Frindt and S. R. Morrison, *Mater. Res. Bull.*, 1986, **21**, 457–461.
- 14 B. Radisavljevic, A. Radenovic, J. Brivio, V. Giacometti and A. Kis, *Nat. Nanotechnol.*, 2011, **6**, 147–150.
- 15 D. Jariwala, V. K. Sangwan, L. J. Lauhon, T. J. Marks and M. C. Hersam, *ACS Nano*, 2014, **8**, 1102–1120.
- 16 J. C. Meyer, A. K. Geim, M. I. Katsnelson, K. S. Novoselov, T. J. Booth and S. Roth, *Nature*, 2007, **446**, 60–63.
- 17 A. Fasolino, J. H. Los and M. I. Katsnelson, *Nat. Mater.*, 2007, **6**, 858–861.
- 18 J. Brivio, D. T. L. Alexander and A. Kis, *Nano Lett.*, 2011, **11**, 5148–5153.
- 19 P. Miro, M. Ghorbani-Asl and T. Heine, *Adv. Mater.*, 2013, **25**, 5473–5475.
- 20 K. S. Novoselov, A. K. Geim, S. V. Morozov, D. Jiang, M. I. Katsnelson, I. V. Grigorieva, S. V. Dubonos and A. A. Firsov, *Nature*, 2005, **438**, 197–200.
- 21 L. F. Sun, J. X. Yan, D. Zhan, L. Liu, H. L. Hu, H. Li, B. K. Tay, J. L. Kuo, C. C. Huang, D. W. Hewak, P. S. Lee and Z. X. Shen, *Phys. Rev. Lett.*, 2013, **111**, 126801.
- 22 Z. Y. Zhu, Y. C. Cheng and U. Schwingenschlogl, *Phys. Rev. B: Condens. Matter Mater. Phys.*, 2011, **84**, 153402.
- 23 W. G. Aulbur, L. Jonsson and J. W. Wilkins, *Solid State Phys.*, 2000, **54**, 1–218.
- 24 L. Hedin, *Phys. Rev.*, 1965, **139**, A796–A823.
- 25 A. P. Cote, A. I. Benin, N. W. Ockwig, M. O'Keeffe, A. J. Matzger and O. M. Yaghi, *Science*, 2005, **310**, 1166–1170.
- 26 R. Dovesi, R. Orlando, B. Civalleri, C. Roetti, V. R. Saunders and C. M. Zicovich-Wilson, *Z. Kristallogr.*, 2005, **220**, 571–573.
- 27 J. M. Soler, E. Artacho, J. D. Gale, A. Garcia, J. Junquera, P. Ordejon and D. Sanchez-Portal, *J. Phys.: Condens. Matter*, 2002, **14**, 2745–2779.
- 28 D. Sanchez-Portal, P. Ordejon and E. Canadell, *Principles and Applications of Density in Inorganic Chemistry II*, 2004, vol. 113, 103–170.
- 29 G. T. Velde and E. J. Baerends, *Phys. Rev. B: Condens. Matter Phys.*, 1991, **44**, 7888–7903.
- 30 G. Wiesenecker and E. J. Baerends, *J. Phys.: Condens. Matter*, 1991, **3**, 6721–6742.
- 31 BAND2013, SCM, *Theoretical Chemistry*, Vrije Universiteit, Amsterdam, The Netherlands.
- 32 P. Giannozzi, S. Baroni, N. Bonini, M. Calandra, R. Car, C. Cavazzoni, D. Ceresoli, G. L. Chiarotti, M. Cococcioni, I. Dabo, A. Dal Corso, S. de Gironcoli, S. Fabris, G. Fratesi, R. Gebauer, U. Gerstmann, C. Gouguassis, A. Kokalj, M. Lazzeri, L. Martin-Samos, N. Marzari, F. Mauri, R. Mazzarello, S. Paolini, A. Pasquarello, L. Paulatto, C. Sbraccia, S. Scandolo, G. Sclauzero, A. P. Seitsonen, A. Smogunov, P. Umari and R. M. Wentzcovitch, *J. Phys.: Condens. Matter*, 2009, **21**, 395502.
- 33 X. Gonze, J. M. Beuken, R. Caracas, F. Detraux, M. Fuchs, G. M. Rignanese, L. Sindic, M. Verstraete, G. Zerah, F. Jollet, M. Torrent, A. Roy, M. Mikami, P. Ghosez, J. Y. Raty and D. C. Allan, *Comput. Mater. Sci.*, 2002, **25**, 478–492.
- 34 X. Gonze, G. M. Rignanese, M. Verstraete, J. M. Beuken, Y. Pouillon, R. Caracas, F. Jollet, M. Torrent, G. Zerah, M. Mikami, P. Ghosez, M. Veithen, J. Y. Raty, V. Olevano, F. Bruneval, L. Reining, R. Godby, G. Onida, D. R. Hamann and D. C. Allan, *Z. Kristallogr.*, 2005, **220**, 558–562.
- 35 X. Gonze, B. Amadon, P. M. Anglade, J. M. Beuken, F. Bottin, P. Boulanger, F. Bruneval, D. Caliste, R. Caracas, M. Cote, T. Deutsch, L. Genovese, P. Ghosez, M. Giantomassi, S. Goedecker, D. R. Hamann, P. Hermet, F. Jollet, G. Jomard, S. Leroux, M. Mancini, S. Mazevet, M. J. T. Oliveira, G. Onida, Y. Pouillon, T. Rangel, G. M. Rignanese, D. Sangalli, R. Shaltaf, M. Torrent, M. J. Verstraete, G. Zerah and J. W. Zwanziger, *Comput. Phys. Commun.*, 2009, **180**, 2582–2615.
- 36 G. Kresse and J. Hafner, *Phys. Rev. B: Condens. Matter Mater. Phys.*, 1993, **47**, 558–561.
- 37 G. Kresse and J. Hafner, *Phys. Rev. B: Condens. Matter Mater. Phys.*, 1994, **49**, 14251–14269.
- 38 G. Kresse and J. Furthmüller, *Phys. Rev. B: Condens. Matter Mater. Phys.*, 1996, **54**, 11169–11186.
- 39 A. Kuc, N. Zibouche and T. Heine, *Phys. Rev. B: Condens. Matter Mater. Phys.*, 2011, **83**, 245213.
- 40 Y. B. Zhang, T. T. Tang, C. Girit, Z. Hao, M. C. Martin, A. Zettl, M. F. Crommie, Y. R. Shen and F. Wang, *Nature*, 2009, **459**, 820–823.

- 41 P. Miró, M. Ghorbani-Asl and T. Heine, *Angew. Chem., Int. Ed.*, 2014, **53**, 3015–3018.
- 42 E. vanLenthe, R. vanLeeuwen, E. J. Baerends and J. G. Snijders, *Int. J. Quantum Chem.*, 1996, **57**, 281–293.
- 43 E. vanLenthe, J. G. Snijders and E. J. Baerends, *J. Chem. Phys.*, 1996, **105**, 6505–6516.
- 44 E. Vanlenthe, E. J. Baerends and J. G. Snijders, *J. Chem. Phys.*, 1994, **101**, 9783–9792.
- 45 E. Vanlenthe, E. J. Baerends and J. G. Snijders, *J. Chem. Phys.*, 1993, **99**, 4597–4610.
- 46 E. van Lenthe, A. Ehlers and E. J. Baerends, *J. Chem. Phys.*, 1999, **110**, 8943–8953.
- 47 W. Koch and M. C. Holthausen, *A Chemist's Guide to Density Functional Theory*, Wiley-VCH, 2001.
- 48 W. Q. Li, C. F. J. Walther, A. Kuc and T. Heine, *J. Chem. Theory Comput.*, 2013, **9**, 2950–2958.
- 49 C. Adamo and V. Barone, *J. Chem. Phys.*, 1999, **110**, 6158–6170.
- 50 J. P. Perdew, K. Burke and M. Ernzerhof, *Phys. Rev. Lett.*, 1996, **77**, 3865–3868.
- 51 J. P. Perdew, K. Burke and M. Ernzerhof, *Phys. Rev. Lett.*, 1997, **78**, 1396.
- 52 Y. Yoon, K. Ganapathi and S. Salahuddin, *Nano Lett.*, 2011, **11**, 3768–3773.
- 53 J. Heyd and G. E. Scuseria, *J. Chem. Phys.*, 2004, **121**, 1187–1192.
- 54 A. Ramasubramaniam, *Phys. Rev. B: Condens. Matter Mater. Phys.*, 2012, **86**, 115409.
- 55 H. L. Shi, H. Pan, Y. W. Zhang and B. I. Yakobson, *Phys. Rev. B: Condens. Matter Mater. Phys.*, 2013, **87**, 155304.
- 56 D. Y. Qiu, F. H. da Jornada and S. G. Louie, *Phys. Rev. Lett.*, 2013, **111**, 216805.
- 57 M. Kuisma, J. Ojanen, J. Enkovaara and T. T. Rantala, *Phys. Rev. B: Condens. Matter Mater. Phys.*, 2010, **82**, 115106.
- 58 M. Ghorbani-Asl, A. N. Enyashin, A. Kuc, T. Heine and G. Seifert, *Phys. Rev. B: Condens. Matter Mater. Phys.*, 2013, 245440–245441.
- 59 S. Datta, *Quantum Transport: Atom to Transistor*, Cambridge University Press, New York, 2nd edn, 2005.
- 60 D. S. Fisher and P. A. Lee, *Phys. Rev. B: Condens. Matter Mater. Phys.*, 1981, **23**, 6851–6854.
- 61 M. P. L. Sancho, J. M. L. Sancho and J. Rubio, *J. Phys. F: Met. Phys.*, 1985, **15**, 851–858.
- 62 A. Sengupta, D. Saha, T. A. Niehaus and S. Mahapatra, 2014, arXiv:1401.4553.
- 63 H. P. Boehm, A. Clauss, G. O. Fischer and U. Hofmann, *Z. Anorg. Chem.*, 1962, **316**, 119–127.
- 64 P. R. Wallace, *Phys. Rev.*, 1947, **71**, 622–634.
- 65 A. K. Geim and K. S. Novoselov, *Nat. Mater.*, 2007, **6**, 183–191.
- 66 Q. Peng, J. Crean, A. K. Dearden, C. Huang, X. D. Wen, S. P. A. Bordas and S. De, *Mod. Phys. Lett. B*, 2013, **27**, 1330017.
- 67 X. D. Wen, T. J. Cahill and R. Hoffmann, *Chem. – Eur. J.*, 2010, **16**, 6555–6566.
- 68 S. Cahangirov, M. Topsakal, E. Akturk, H. Sahin and S. Ciraci, *Phys. Rev. Lett.*, 2009, **102**, 236804.
- 69 B. Aufray, A. Kara, S. Vizzini, H. Oughaddou, C. Leandri, B. Ealet and G. Le Lay, *Appl. Phys. Lett.*, 2010, **96**, 183102.
- 70 B. J. Feng, Z. J. Ding, S. Meng, Y. G. Yao, X. Y. He, P. Cheng, L. Chen and K. H. Wu, *Nano Lett.*, 2012, **12**, 3507–3511.
- 71 H. Jamgotchian, Y. Colignon, N. Hamzaoui, B. Ealet, J. Y. Hoarau, B. Aufray and J. P. Biberian, *J. Phys.: Condens. Matter*, 2012, **24**, 172001.
- 72 J. F. Dienstmaier, D. D. Medina, M. Dogru, P. Knochel, T. Bein, W. M. Heckl and M. Lackinger, *ACS Nano*, 2012, **6**, 7234–7242.
- 73 P. Vogt, P. De Padova, C. Quaresima, J. Avila, E. Frantzeskakis, M. C. Asensio, A. Resta, B. Ealet and G. Le Lay, *Phys. Rev. Lett.*, 2012, **108**, 155501.
- 74 S. Cahangirov, M. Audiffred, P. Z. Tang, A. Iacomino, W. H. Duan, G. Merino and A. Rubio, *Phys. Rev. B: Condens. Matter Mater. Phys.*, 2013, **88**, 035432.
- 75 A. Fleurence, R. Friedlein, T. Ozaki, H. Kawai, Y. Wang and Y. Yamada-Takamura, *Phys. Rev. Lett.*, 2012, **108**, 245501.
- 76 L. Meng, Y. L. Wang, L. Z. Zhang, S. X. Du, R. T. Wu, L. F. Li, Y. Zhang, G. Li, H. T. Zhou, W. A. Hofer and H. J. Gao, *Nano Lett.*, 2013, **13**, 685–690.
- 77 L. Liu, Y. P. Feng and Z. X. Shen, *Phys. Rev. B: Condens. Matter Mater. Phys.*, 2003, **68**, 104102.
- 78 Effective masses calculated assuming a parabolic behaviour of top and bottom of valence and conduction bands, respectively.
- 79 A. Pakdel, Y. Bando and D. Golberg, *Chem. Soc. Rev.*, 2014, **43**, 934–959.
- 80 G. Constantinescu, A. Kuc and T. Heine, *Phys. Rev. Lett.*, 2013, **111**, 036104.
- 81 H. Sahin, S. Cahangirov, M. Topsakal, E. Bekaroglu, E. Akturk, R. T. Senger and S. Ciraci, *Phys. Rev. B: Condens. Matter Mater. Phys.*, 2009, **80**, 155453.
- 82 J. C. Garcia, D. B. de Lima, L. V. C. Assali and J. o. F. Justo, *J. Phys. Chem. C*, 2011, **115**, 13242–13246.
- 83 P. Gori, O. Pulci, M. Marsili and F. Bechstedt, *Appl. Phys. Lett.*, 2012, **100**, 261906.
- 84 X. Y. Huang and J. Li, *J. Am. Chem. Soc.*, 2007, **129**, 3157–3162.
- 85 J. S. Son, X. D. Wen, J. Joo, J. Chae, S. I. Baek, K. Park, J. H. Kim, K. An, J. H. Yu, S. G. Kwon, S. H. Choi, Z. W. Wang, Y. W. Kim, Y. Kuk, R. Hoffmann and T. Hyeon, *Angew. Chem., Int. Ed.*, 2009, **48**, 6861–6864.
- 86 S. Ithurria, M. D. Tessier, B. Mahler, R. P. S. M. Lobo, B. Dubertret and A. Efros, *Nat. Mater.*, 2011, **10**, 936–941.
- 87 C. Tusche, H. L. Meyerheim and J. Kirschner, *Phys. Rev. Lett.*, 2007, **99**, 026102.
- 88 G. Weirum, G. Barcaro, A. Fortunelli, F. Weber, R. Schennach, S. Surnev and F. P. Netzer, *J. Phys. Chem. C*, 2010, **114**, 15432–15439.
- 89 J. Zhou, J. S. Huang, B. G. Sumpter, P. R. C. Kent, H. Terrones and S. C. Smith, *J. Phys. Chem. C*, 2013, **117**, 26858.
- 90 J. Zhou, J. S. Huang, B. G. Sumpter, P. R. C. Kent, H. Terrones and S. C. Smith, *J. Phys. Chem. C*, 2013, **117**, 25817–25825.

- 91 E. Bianco, S. Butler, S. S. Jiang, O. D. Restrepo, W. Windl and J. E. Goldberger, *ACS Nano*, 2013, **7**, 4414–4421.
- 92 K. J. Koski and Y. Cui, *ACS Nano*, 2013, **7**, 3739–3743.
- 93 R. R. Nair, W. C. Ren, R. Jalil, I. Riaz, V. G. Kravets, L. Britnell, P. Blake, F. Schedin, A. S. Mayorov, S. J. Yuan, M. I. Katsnelson, H. M. Cheng, W. Strupinski, L. G. Bulusheva, A. V. Okotrub, I. V. Grigorieva, A. N. Grigorenko, K. S. Novoselov and A. K. Geim, *Small*, 2010, **6**, 2877–2884.
- 94 D. K. Samarakoon, Z. F. Chen, C. Nicolas and X. Q. Wang, *Small*, 2011, **7**, 965–969.
- 95 Y. Ding and Y. L. Wang, *Appl. Phys. Lett.*, 2012, **100**, 083102.
- 96 M. Chhowalla, H. S. Shin, G. Eda, L. J. Li, K. P. Loh and H. Zhang, *Nat. Chem.*, 2013, **5**, 263–275.
- 97 F. L. Claus, *Solid Lubricants and Self-Lubricating Solids*, Academic Press, New York, 1972.
- 98 C. Ataca, H. Sahin and S. Ciraci, *J. Phys. Chem. C*, 2012, **116**, 8983–8999.
- 99 N. Zibouche, P. Philipsen, A. Kuc and T. Heine, *Phys. Chem. Chem. Phys.*, 2014, DOI: 10.1039/C4CP00966E.
- 100 A. Splendiani, L. Sun, Y. Zhang, T. Li, J. Kim, C.-Y. Chim, G. Galli and F. Wang, *Nano Lett.*, 2010, **10**, 1271–1275.
- 101 G. Eda, H. Yamaguchi, D. Voiry, T. Fujita, M. Chen and M. Chhowalla, *Nano Lett.*, 2011, **11**, 5111–5116.
- 102 H. R. Gutiérrez, N. Perea-López, A. L. Elías, A. Berkdemir, B. Wang, R. Lv, F. López-Urías, V. H. Crespi, H. Terrones and M. Terrones, *Nano Lett.*, 2012, **13**, 3447–3454.
- 103 S. Bertolazzi, D. Krasnozhon and A. Kis, *ACS Nano*, 2013, **7**, 3246–3252.
- 104 B. Radisavljevic and A. Kis, *Nat. Mater.*, 2013, **12**, 815–820.
- 105 H. Y. Chang, S. X. Yang, J. H. Lee, L. Tao, W. S. Hwang, D. Jena, N. S. Lu and D. Akinwande, *ACS Nano*, 2013, **7**, 5446–5452.
- 106 G. H. Lee, Y. J. Yu, X. Cui, N. Petrone, C. H. Lee, M. S. Choi, D. Y. Lee, C. Lee, W. J. Yoo, K. Watanabe, T. Taniguchi, C. Nuckolls, P. Kim and J. Hone, *ACS Nano*, 2013, **7**, 7931–7936.
- 107 J. Yoon, W. Park, G. Y. Bae, Y. Kim, H. S. Jang, Y. Hyun, S. K. Lim, Y. H. Kahng, W. K. Hong, B. H. Lee and H. C. Ko, *Small*, 2013, **9**, 3295–3300.
- 108 N. Scheuschner, O. Ochedowski, M. Schleberger and J. Maultzsch, *Phys. Status Solidi B*, 2012, **249**, 2644–2647.
- 109 S. Bertolazzi, J. Brivio and A. Kis, *ACS Nano*, 2011, **5**, 9703–9709.
- 110 M. Ghorbani-Asl, S. Borini, A. Kuc and T. Heine, *Phys. Rev. B: Condens. Matter Mater. Phys.*, 2013, **87**, 235434.
- 111 K. Roy, M. Padmanabhan, S. Goswami, T. P. Sai, G. Ramalingam, S. Raghavan and A. Ghosh, *Nat. Nanotechnol.*, 2013, **8**, 826–830.
- 112 Z. M. Wang, *MoS₂ Materials, Physics, and Devices*, Springer, 2014.
- 113 O. Lopez-Sanchez, D. Lembke, M. Kayci, A. Radenovic and A. Kis, *Nat. Nanotechnol.*, 2013, **8**, 497–501.
- 114 J. H. Han, S. Lee and J. Cheon, *Chem. Soc. Rev.*, 2013, **42**, 2581–2591.
- 115 S. Jeong, D. Yoo, J. T. Jang, M. Kim and J. Cheon, *J. Am. Chem. Soc.*, 2012, **134**, 18233–18236.
- 116 J. T. Jang, S. Jeong, J. W. Seo, M. C. Kim, E. Sim, Y. Oh, S. Nam, B. Park and J. Cheon, *J. Am. Chem. Soc.*, 2011, **133**, 7636–7639.
- 117 S. Jeong, J. H. Han, J. T. Jang, J. W. Seo, J. G. Kim and J. Cheon, *J. Am. Chem. Soc.*, 2011, **133**, 14500–14503.
- 118 S. Furuseth, K. Selte and A. Kjekshus, *Acta Chem. Scand.*, 1965, **19**, 257.
- 119 Y. D. Ma, Y. Dai, M. Guo, L. Yu and B. B. Huang, *Phys. Chem. Chem. Phys.*, 2013, **15**, 7098–7105.
- 120 H. Hillebrecht, P. J. Schmidt, H. W. Rotter, G. Thiele, P. Zonnchen, H. Bengel, H. J. Cantow, S. N. Magonov and M. H. Whangbo, *J. Alloys Compd.*, 1997, **246**, 70–79.
- 121 D. Shriver and P. Atkins, *Inorganic Chemistry*, W. H. Freeman, 2009.
- 122 S. Kandambeth, D. B. Shinde, M. K. Panda, B. Lukose, T. Heine and R. Banerjee, *Angew. Chem., Int. Ed.*, 2013, **52**, 13052–13056.
- 123 S. Chandra, S. Kandambeth, B. P. Biswal, B. Lukose, S. M. Kunjir, M. Chaudhary, R. Babarao, T. Heine and R. Banerjee, *J. Am. Chem. Soc.*, 2013, **135**, 17853–17861.
- 124 B. P. Biswal, S. Chandra, S. Kandambeth, B. Lukose, T. Heine and R. Banerjee, *J. Am. Chem. Soc.*, 2013, **135**, 5328–5331.
- 125 S. Kandambeth, A. Mallick, B. Lukose, M. V. Mane, T. Heine and R. Banerjee, *J. Am. Chem. Soc.*, 2012, **134**, 19524–19527.
- 126 B. Lukose, A. Kuc and T. Heine, *Chem. – Eur. J.*, 2011, **17**, 2388–2392.
- 127 L. R. Xu, X. Zhou, Y. X. Yu, W. Q. Tian, J. Ma and S. B. Lei, *ACS Nano*, 2013, **7**, 8066–8073.
- 128 B. Lukose, A. Kuc, J. Frenzel and T. Heine, *Beilstein J. Nanotechnol.*, 2010, **1**, 60–70.
- 129 J. V. Lauritsen, J. Kibsgaard, S. Helveg, H. Topsoe, B. S. Clausen, E. Laegsgaard and F. Besenbacher, *Nat. Nanotechnol.*, 2007, **2**, 53–58.
- 130 S. H. Vosko, L. Wilk and M. Nusair, *Can. J. Phys.*, 1980, **58**, 1200–1211.
- 131 Y. Zhao and D. G. Truhlar, *J. Chem. Phys.*, 2006, **125**, 194101.
- 132 C. Bouet, M. D. Tessier, S. Ithurria, B. Mahler, B. Nadal and B. Dubertret, *Chem. Mater.*, 2013, **24**, 1262–1271, DOI: 10.1021/cm303786a.